JOINT TRANSPORTATION
RESEARCH PROGRAM
INDIANA DEPARTMENT OF TRANSPORTATION
AND PURDUE UNIVERSITY

Road Ditch Line Mapping with Mobile LiDAR

Ayman Habib, Darcy Bullock, Yi-Chun Lin, Raja Manish

SPR-4407 • Report Number: FHWA/IN/JTRP-2021/26 • DOI: 10.5703/1288284317354

RECOMMENDED CITATION

Habib, A., Bullock, D. M., Lin, Y.-C., & Manish, R. (2021). *Road ditch line mapping with mobile LiDAR* (Joint Transportation Research Program Publication No. FHWA/IN/JTRP-2021/26). West Lafayette, IN: Purdue University. https://doi.org/10.5703/1288284317354

AUTHORS

Ayman Habib, PhD
Thomas A. Page Professor in Civil Engineering
Lyles School of Civil Engineering
(765) 496-0173
ahabib@purdue.edu
Corresponding Author

Darcy M. Bullock, PhD, PE
Lyles Family Professor of Civil Engineering
Lyles School of Civil Engineering
Purdue University

Yi-Chun Lin
Graduate Research Assistant
Lyles School of Civil Engineering
Purdue University

Raja Manish
Graduate Research Assistant
Lyles School of Civil Engineering
Purdue University

JOINT TRANSPORTATION RESEARCH PROGRAM

The Joint Transportation Research Program serves as a vehicle for INDOT collaboration with higher education institutions and industry in Indiana to facilitate innovation that results in continuous improvement in the planning, design, construction, operation, management and economic efficiency of the Indiana transportation infrastructure. https://engineering.purdue.edu/JTRP/index_html

Published reports of the Joint Transportation Research Program are available at http://docs.lib.purdue.edu/jtrp/.

NOTICE

TECHNICAL REPORT DOCUMENTATION PAGE

1. Report No. FHWA/IN/JTRP-2021/26	**2. Government Accession No.**	**3. Recipient's Catalog No.**
4. Title and Subtitle Road Ditch Line Mapping with Mobile LiDAR		**5. Report Date** July 2021 **6. Performing Organization Code**
7. Author(s) Ayman Habib, Darcy M. Bullock, Yi-Chun Lin, and Raja Manish		**8. Performing Organization Report No.** FHWA/IN/JTRP-2021/26
9. Performing Organization Name and Address Joint Transportation Research Program Hall for Discovery and Learning Research (DLR), Suite 204 207 S. Martin Jischke Drive West Lafayette, IN 47907		**10. Work Unit No.** **11. Contract or Grant No.** SPR-4407
12. Sponsoring Agency Name and Address Indiana Department of Transportation (SPR) State Office Building 100 North Senate Avenue Indianapolis, IN 46204		**13. Type of Report and Period Covered** Final Report **14. Sponsoring Agency Code**
15. Supplementary Notes Conducted in cooperation with the U.S. Department of Transportation, Federal Highway Administration.		

16. Abstract

Maintenance of roadside ditches is important to avoid localized flooding and premature failure of pavements. Scheduling effective preventative maintenance requires mapping of the ditch profile to identify areas requiring excavation of long-term sediment accumulation. High-resolution, high-quality point clouds collected by mobile LiDAR mapping systems (MLMS) provide an opportunity for effective monitoring of roadside ditches and performing hydrological analyses. This study evaluated the applicability of mobile LiDAR for mapping roadside ditches for slope and drainage analyses. The performance of alternative MLMS units was performed. These MLMS included an unmanned ground vehicle, an unmanned aerial vehicle, a portable backpack system along with its vehicle-mounted version, a medium-grade wheel-based system, and a high-grade wheel-based system. Point cloud from all the MLMS units were in agreement in the vertical direction within the ±3 cm range for solid surfaces, such as paved roads, and ±7 cm range for surfaces with vegetation. The portable backpack system that could be carried by a surveyor or mounted on a vehicle and was the most flexible MLMS. The report concludes that due to flexibility and cost effectiveness of the portable backpack system, it is the preferred platform for mapping roadside ditches, followed by the medium-grade wheel-based system.

Furthermore, a framework for ditch line characterization is proposed and tested using datasets acquired by the medium-grade wheel-based and vehicle-mounted portable systems over a state highway. An existing ground filtering approach is modified to handle variations in point density of mobile LiDAR data. Hydrological analyses, including flow direction and flow accumulation, are applied to extract the drainage network from the digital terrain model (DTM). Cross-sectional/longitudinal profiles of the ditch are automatically extracted from LiDAR data and visualized in 3D point clouds and 2D images. The slope derived from the LiDAR data was found to be very close to highway cross slope design standards of 2% on driving lanes, 4% on shoulders, as well as 6-by-1 slope for ditch lines. Potential flooded regions are identified by detecting areas with no LiDAR return and a recall score of 54% and 92% was achieved by the medium-grade wheel-based and vehicle-mounted portable systems, respectively.

17. Key Words LiDAR, mobile mapping system, digital terrain model generation, slope analysis, longitudinal/cross-sectional profiles, roadside ditch, drainage network	**18. Distribution Statement** No restrictions. This document is available through the National Technical Information Service, Springfield, VA 22161.

19. Security Classif. (of this report) Unclassified	**20. Security Classif. (of this page)** Unclassified	**21. No. of Pages** 33	**22. Price**

EXECUTIVE SUMMARY

Introduction

Roadside ditches are designed to minimize local flooding risk by draining water away from the roadway. In addition to transporting road runoff, roadside ditches play a critical role in the transport of pollutants and the increase in peak storm flows since they substantially alter natural flow pathways and routing efficiencies. An improved management of roadside ditches is not only crucial to roadway maintenance but also lays the foundation for assessing their impact on the natural hydrologic and nutrient transport network. While ditch networks are being increasingly incorporated in distributed hydrologic modeling, the ability to accurately extract drainage networks from remote sensing data remains challenging. Specifically, high-resolution, large-scale data that can capture the ditches, often narrow and covered by vegetation, through an efficient field survey is the current bottleneck.

Mobile LiDAR Mapping Systems (MLMS) have witnessed tremendous growth of their applications in the field of remote sensing. Such systems are capable of collecting high-quality, dense point clouds in an efficient manner. Mapping ditches using high-resolution LiDAR can be a cost-effective alternative to field surveys for prioritizing and planning ditch maintenance. It also eliminates the unnecessary exposure of survey crews to work hazards in traffic zones. This study assesses the feasibility of using mobile LiDAR techniques for mapping roadside ditches for slope and drainage network analyses. The following research aims are addressed: (1) evaluate the ability of different MLMS grades to provide quantitative measures of the condition of roadside ditches and (2) develop data processing strategies for characterizing the ditch lines.

Findings

- The performance of different grades of MLMS units was assessed in terms of spatial coverage, relative vertical accuracy, and absolute vertical accuracy. These MLMS units included an unmanned ground vehicle, an unmanned aerial vehicle, a portable Backpack system along with its vehicle-mounted version, a medium-grade wheel-based system, and a high-grade wheel-based system.
- Point cloud from all the MLMS units agreed within the ± 3 cm range for solid surfaces, such as paved roads, and ± 7 cm range for surfaces with vegetation along the vertical direction.
- The portable Backpack system that could be carried by a surveyor or mounted on a vehicle was the most flexible MLMS for mapping roadside ditches, followed by the medium-grade wheel-based system.
- The cross-sectional/longitudinal profiles of the ditch were automatically extracted from LiDAR data and visualized both in 2D image and 3D point cloud.
- The slope derived from the LiDAR data was found to be very close to highway cross slope design standards of 2% on driving lanes, 4% on shoulder, as well as a 6-by-1 slope for ditch lines.
- Potential flooded regions are identified and visualized both in point cloud and images. A recall score of 54% and 92% was achieved by the medium-grade wheel-based and vehicle-mounted portable systems, respectively.

Implementation

- *System calibration:* The relative position and orientation (hereafter denoted as mounting parameters) between the LiDAR and imaging sensors and the GNSS/INS unit are estimated using an in-situ calibration procedure. This procedure estimates the mounting parameters by minimizing discrepancies among conjugate points, linear features, and/or planar features obtained from different LiDAR units and cameras in different drive-runs/flight lines.
- *Ground filtering:* A ground filtering approach adapted from the cloth simulation algorithm is proposed to separate bare earth points from above-ground points. First, the original cloth simulation approach is used to extract the bare earth point cloud. Next, the rigidness of the cloth is redefined based on the point density of the bare earth point cloud. Finally, the cloth simulation is applied again to obtain a refined bare earth point cloud and the final digital terrain model (DTM).
- *Cross-sectional profile extraction:* A cross-sectional profile with a given length and width can be extracted from the point cloud, bare earth point cloud, and/or DTM at any location. The orientation of the profile should be perpendicular to the direction of the road, which is derived using the vehicle trajectory information. Once the profile is extracted, the slope along the profile is evaluated using the bare earth points. The results are visualized in both 3D point clouds and 2D images.
- *Drainage network and longitudinal profile extraction:* The drainage network is identified by calculating the flow direction and flow accumulation using the DTM. A longitudinal profile is the one along the "valley" of a ditch. It is identified by removing tributaries and connecting major streams of the drainage network.
- *Potential flooded region detection and visualization:* Potential flooded regions can be identified by detecting areas where the LiDAR points are absent. First, a binary point density image over the region of interest is generated. A median filter is then applied to reduce the noise caused by irregular point distribution. Next, the boundary between the black and white cells is traced. A region of interest is reported if its area is larger than a user-defined threshold. The reported regions of interest are visualized both in 3D point cloud and 2D images.
- *MLMS units:* The MLMS units as well as data acquisition and processing strategies developed by the research team can collect information of existing ditch geometry with efficient field surveys. The tool can be used for comparison between planned-built and existing ditch geometries at a network and project level for the INDOT.

CONTENTS

LIST OF TABLES

LIST OF FIGURES

1. INTRODUCTION

Roadside ditches are designed to minimize local flooding risk by draining water away from the roadway. In addition to transporting road runoff, roadside ditches play a critical role in the transport of pollutants and the increase in peak storm flows since they substantially alter the natural flow pathways and routing efficiencies (Buchanan et al., 2013; Schneider et al., 2019). An improved management of roadside ditches is not only crucial to roadway maintenance, but also lays the foundation for assessing their impact on the natural hydrologic and nutrient transport network. While ditch networks are being increasingly incorporated in distributed hydrologic modeling, the ability to accurately extract drainage networks from remote sensing data remains challenging (Ariza-Villaverde et al., 2015; Levavasseur et al., 2015; Metz et al., 2011; Roelens, Höfle, et al., 2018). Specifically, high-resolution, large-scale data that can capture the ditches, often narrow and covered by vegetation, through an efficient field survey is the current bottleneck. Previous studies have identified the lack of maintenance of roadside ditches due to limited resources including time, labor, equipment, and funding (Schneider et al., 2019). It was noted that an estimated one-third to one-half of the ditches in New York State were in fair to poor condition (Schneider et al., 2019). Advancements in remote sensing data acquisition, processing, and analysis facilitate the investigation of the hydrological effects of roadside ditches and benefit ditch maintenance practices.

Mobile LiDAR mapping systems (MLMS) have witnessed tremendous growth of their applications in the field of remote sensing. Such systems are capable of collecting high-quality, dense point clouds in an efficient manner. Previous studies reported on the use of MLMS for automated lane marking detection (Cheng et al., 2020; Wen et al., 2019), runway grade evaluation (Lin et al., 2019), and debris/pavement distress inspection (Ravi et al., 2020). Mapping ditches using high-resolution LiDAR can be a cost-effective alternative to field surveys for prioritizing and planning ditch maintenance. It also eliminates the unnecessary exposure of survey crews to work hazards in traffic zones. This study assesses the feasibility of using mobile LiDAR techniques for mapping roadside ditches for slope and drainage network analyses. The following research aims are addressed: (1) evaluate the ability of different MLMS grades to provide quantitative measures of the condition of roadside ditches; and (2) develop data processing strategies for characterizing ditch lines. The rest of the report is structured as follows: Section 2 provides an overview of prior research related to mapping natural streams and man-made ditches; Section 3 describes the data acquisition systems and field surveys; Section 4 introduces the proposed ditch line characterization strategies; Section 5 presents the experimental results and discussion; Section 6 summarizes the research key findings and provides directions for future work.

2. RELATED WORK

Remote sensing techniques, including satellite and aerial imagery as well as airborne LiDAR, have been the dominant tool for mapping natural stream networks and man-made drainage ditches. While most of the major rivers can be properly mapped, the challenge lies in capturing narrow streams and man-made ditches. Levavassur et al. (2012; 2015) conducted exhaustive field surveys of man-made drainage networks to investigate the extent to which drainage density depends on agricultural landscape attributes such as topography and soil type. While aerial photographs assisted in locating elements of the drainage network, the authors noted that remote sensing data may not be accurate enough to map ditches that are less than a meter wide (Levavasseur et al., 2015). Hydrological analyses are common approaches for automated drainage network extraction. Such analyses typically require a digital terrain model (DTM) derived from remote sensing data. A DTM can be generated from airborne LiDAR data (Barber & Shortridge, 2005; Bertels et al., 2011; Ibeh et al., n.d.; Murphy et al., 2007), airborne photogrammetric data (Ariza-Villaverde et al., 2015; Murphy et al., 2007), spaceborne radar data (Metz et al., 2011), UAV photogrammetric data (Günen et al., 2019), and most recently, UAV LiDAR data (Pricope et al., 2020). Then, the stream network can be extracted by calculating the flow direction and flow accumulation for each DTM cell and using a threshold to determine DTM cells that represent streamlines. All these studies suggest that using high-resolution DTM provides more accurate results, especially when the drainage network is dense.

Although most of the existing literature has highlighted the importance of LiDAR in generating elevation models, only a few have focused on characterizing ditches. In one of the early efforts, Bailly et al. (2008) utilized LiDAR-derived elevation profiles and carried out curve shape analysis to detect and classify any concavity within the elevation profiles as a ditch or non-ditch entity. The ditch detection results were validated through ground surveys. A high omission rate was observed due to vegetation covering ditches or the LiDAR data not being dense enough. Rapinel et al. (2015) derived DTMs from airborne LiDAR data with different point densities and used an object-based image analysis approach for drainage network extraction. The focus was to estimate ditch depth and the results were validated by field measurements collected by a total station. Their results showed that if the point density fell below two points per square meter, the ditch depth could become underestimated. Moreover, the quality of the generated drainage network map depends primarily on the point density of LiDAR data rather than the interpolation method used for DTM generation. Instead of using DTM, Broersen et al. (2017) used classified airborne LiDAR point cloud to detect drainage networks. Two approaches were proposed: 2D skeleton and 3D skeleton. The former took advantage of the

property that LiDAR has no return over water bodies, and detected ditches filled with water by finding the concave hull of the ground and vegetation points. The latter utilized the 3D morphology of the landscape to identify ditches that are dry or covered by canopy. One of the limitations of this study is the tendency to find and classify unexpected concavities as watercourse. Roelens et al. (Roelens, Höfle, et al., 2018; Roelens, Rosier, et al., 2018) extracted drainage ditches directly from irregular airborne LiDAR point clouds with an average point spacing of 0.10 m instead of interpolated DTM. The LiDAR points were classified as ditch and non-ditch points using a random forest classifier. Their approach requires radiometric features (RGB, intensity, and vegetation indices) for improved results in grasslands.

Previous studies suggested that the ground sampling distance of the DTM or the inter-point spacing of the LiDAR data is critical for ensuring the quality of ditch mapping. The point density of airborne systems may not be adequate to capture man-made drainage ditches, which can be very narrow and densely covered with vegetation. This study utilizes ground-based MLMS units which have a much higher point density and accuracy when compared to airborne systems for mapping roadside drainage ditches. Moreover, ditch line characterization strategies using LiDAR data are developed.

3. DATA ACQUISITION SYSTEMS AND DATASET DESCRIPTION

This section starts with an introduction of the platform architecture, sensor integration, and system calibration of the MLMS units used in this study. Further, we provide information regarding the field surveys and acquired datasets.

3.1 Specifications of Different MLMS Units

A total of six mobile mapping systems are used in this study: an unmanned aerial vehicle (UAV), an unmanned ground vehicle (UGV), a Backpack-mounted portable system (hereafter called Backpack), the portable system mounted on a carrier vehicle (hereafter called Mobile-pack), a medium-grade wheel-based system: Purdue wheel-based mobile mapping system–high accuracy (PWMMS-HA), and a high-grade wheel-based system: Purdue wheel-based mobile mapping system—ultra-high accuracy (PWMMS-UHA). All the six MLMS units are shown in Figure 3.1.

The UAV (shown in Figure 3.1a) payload consists of a Velodyne VLP-32C LiDAR and a Sony 43.6 MP full-frame camera with a 35 mm lens. The LiDAR and the camera are directly georeferenced by an Applanix APX15v3 position and orientation unit integrating global navigation satellite systems/inertial navigation systems (GNSS/INS). More specifically, the position and orientation information of the two sensors at any point during surveys are directly obtained by the GNSS/INS unit. The UGV (shown in Figure 3.1b) consists of a Velodyne VLP-16 Hi-Res 16 beam LiDAR unit and a Sony 36.3 MP full-frame camera with an 8 mm lens. The LiDAR data and images from the camera are georeferenced by a NovAtel SPAN-IGM GNSS/INS unit. The Backpack system is comprised of a VLP-16 Hi-Res LiDAR and a Sony 42.4 MP full-frame camera with a 35 mm lens. These two sensors are georeferenced by a NovAtel SPAN-CPT GNSS/INS unit. This Backpack system has the versatility of either being worn by a survey crew, as depicted in Figure 3.1c, for off-road data acquisition, or be mounted on a carrier vehicle for scanning long corridors, as shown in Figure 3.1d. The PWMMS-HA is equipped with four LiDAR units: three Velodyne HDL-32E and one Velodyne VLP-16 High-Res, three FLIR Grasshopper3 9.1 MP GigE color cameras with an 8 mm lens (Figure 3.1e). All the sensors are georeferenced by an Applanix POS LV 220 GNSS/INS unit. The PWMMS-UHA, as shown in Figure 3.1f, carries two profiling LiDAR units—a Riegl VUX 1HA and a Z+F Profiler 9012. There are also two rear-facing FLIR Flea2 FireWire color cameras with a 12 mm lens. These LiDAR and RGB camera units are georeferenced by a NovAtel ProPak6 GNSS receiver and ISA-100C near-navigation grade IMU. Table 3.1 lists the specifications of the georeferencing (Applanix, n.d.a; n.d.b; Hexagon, n.d.a; n.d.b; 2021) and LiDAR units (Riegl, n.d.; Velodyne, n.d.a; n.d.b; n.d.c; Zoller + Frolich, n.d.) for each MLMS including the approximate total cost of the equipment.

The RGB cameras on each MLMS are triggered at a periodic interval through different instrumentation setups. The three FLIR cameras onboard PWMMS-HA are triggered using pulse output from POS LV as an input to the cameras. For all other MLMS units, a separate hardware circuit is utilized that triggers their cameras at a fixed time interval (once every few seconds). Image capture events are logged by the GNSS/INS unit of each platform. Using GNSS for event logging ensures that the time of capture is accurately tagged using the precise GNSS receiver clock.

While the specifications of a LiDAR sensor are critical in determining the resulting point cloud density, sensor orientation and sensor-to-object distance play an important role in defining the most relevant field of view which provides the highest number of beam returns from a given region of interest (ROI). The UAV system is built in a way that the rotation axis of the LiDAR unit is approximately parallel to the flying direction. The UGV LiDAR unit, owing to its tilt and proximity to the ground, produces a highly dense point cloud, but the useful scan area is limited to a very small field of view. The Backpack system has a similar orientation of its LiDAR unit as that of the UGV; however, the unit, being positioned at least a meter above the ground, enables scanning a large surface area for the same angle subtended at the LiDAR unit as that of the UGV. The LiDAR sensors onboard the PWMMS-HA have only a slight tilt towards the ground, meaning each sensor covers a very large

ground surface area. One would expect the resulting point cloud from PWMMS-HA to be sparse. On the contrary, as an advantage of having multiple sensors on the platform, any sparsity of points due to the large ground scan area is compensated by the additional LiDAR units through accurate system calibration. In case of the PWMMS-UHA, which is outfitted with two high-precision profiler LiDAR units, the sensors have similar tilts as the UGV. Additionally, the high pulse repetition rates of the LiDAR units allow for obtaining a high-density point cloud of the ground surface. Thus, selecting a suitable MLMS with an optimal sensor configuration is the key to deriving high density point cloud for a detailed mapping of roadside ditches from the acquired LiDAR data.

3.2 System Calibration of Different MLMS units

The raw data collected by various MLMS units includes LiDAR range and intensity measurements, camera images, and georeferencing information from the GNSS/INS unit. In order to reconstruct accurately geo-referenced and well-registered point cloud as well as to integrate the information from cameras, a system calibration procedure that estimates the relative position and orientation (hereafter, denoted as mounting parameters) between the LiDAR and imaging sensors and the GNSS/INS unit is required. The mounting parameters in this study are accurately estimated using the in-situ calibration procedure proposed by Ravi et al. (2018). This procedure estimates the mounting parameters by minimizing discrepancies among conjugate points, linear features, and/or planar features obtained from different LiDAR units and cameras in different drive-runs/flight lines. Table 3.2 shows the range of standard deviation of estimated mounting parameters for all LiDAR units/cameras onboard each MLMS from the system calibration. The lever arm component along the Z direction (ΔZ) was determined by incorporating RTK-GNSS survey measurements in

Figure 3.1 *Continued.*

(d)

(e)

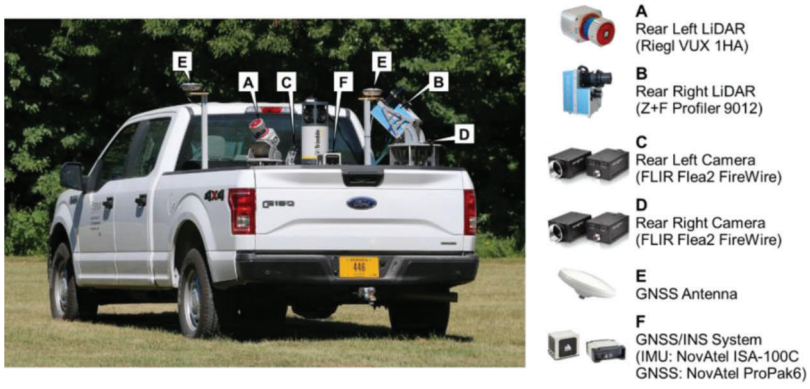

(f)

Figure 3.1 MLMS units used in this study: (a) unmanned aerial vehicle (UAV), (b) unmanned ground vehicle (UGV), (c) Backpack, (d) Mobile-pack, (e) medium-grade system (PWMMS-HA), and (f) high-grade system (PWMMS-UHA). All of these platforms are non-commercial systems designed and integrated by the research group.

the calibration model as vertical control. The accuracy of the final ground coordinates for each MLMS at a specified sensor-to-object distance was evaluated using the LiDAR Error Propagation calculator developed by Habib et al. (2006). The results, as shown in Table 3.3, indicate that an accuracy of under 5–6 cm is achievable from all systems.

Once the mounting parameters are estimated accurately, the LiDAR point clouds and images captured by individual sensors onboard the systems can be directly georeferenced to a common reference frame. More specifically, using the estimated mounting parameters, together with the GNSS/INS trajectory, one can (1) reconstruct a georeferenced LiDAR point cloud, and (2) obtain the position and orientation of the camera in a global mapping frame whenever an image is captured. This capability allows for a forward and backward projection between the reconstructed point cloud and camera imagery. Thus, an ROI in the point cloud can be identified and projected to images containing those points. Such image-LiDAR integration facilitates qualitative reporting of ditch mapping/characterization, i.e., the ditches can be visualized and reported in 3D point clouds as well as 2D images even though they are mainly detected and mapped in 3D space. The image-based visualization is useful for

TABLE 3.1
Specifications of the georeferencing and LiDAR sensors for each MLMS, including the approximate total cost

	UAV	UGV	Backpack/Mobile-Pack	PWMMS-HA		PWMMS-UHA	
GNSS/INS Sensors	Applanix APX15v3	NovAtel SPAN-IGM-S1	NovAtel SPAN-CPT	Applanix POS LV 220		NovAtel ProPak6; IMU-ISA-100C	
Sensor Weight	0.06 kg	0.54 kg	2.28 kg	2.40 + 2.50 kg		1.79 + 5.00 kg	
Positional Accuracy	2–5 cm	2–3 cm	1–2 cm	2–5 cm		1–2 cm	
Attitude Accuracy (Roll/Pitch)	0.025	0.006	0.015	0.015		0.003	
Attitude Accuracy (Heading)	0.08	0.02	0.03	0.025		0.004	
LiDAR Sensors	Velodyne VLP-32C	Velodyne VLP-16 High-Res	Velodyne VLP-16 High-Res	Velodyne VLP-16 High-Res	Velodyne HDL-32E	Riegl VUX 1HA	Z+F Profiler 9012
Sensor Weight	0.925 kg	0.830 kg	0.830 kg	0.830 kg	1.0 kg	3.5 kg	13.5 kg
No. of Channels	32	16	16	16	32	1	1
Pulse Repetition Rate	600,000 point/s (single return)	~300,000 point/s (single return)	~300,000 point/s (single return)	~300,000 point/s (single return)	~695,000 point/s (single return)	Up to 1,000,000 point/s	Up to 1,000,000 point/s
Maximum Range	200 m	100 m	100 m	100 m	100 m	135 m	119 m
Range Accuracy	±3 cm	±3 cm	±3 cm	±3 cm	±2 cm	±5 mm	±2 mm
MLMS Cost (USD)	~$60,000	~$37,000	~$36,000	~$190,000		~$320,000	

effective mitigation of detected problems during the ditch mapping (e.g., deviation from the design profile of the ditch, improper grade along the ditch, and debris within the ditch).

3.3 Dataset Description

A total of ten datasets were collected by different mobile LiDAR mapping systems over three study sites. Table 3.4 lists the drive-run/flight configuration of each dataset. The performance of ground-based MLMS units for mapping roadside ditches is assessed against one of the well-studied aerial data acquisition methods, UAV, using datasets A-1, A-2, and A-3. Datasets B-1 to B-5 are used to evaluate the comparative performance between different ground-based MLMS units and identify the most practical ditch mapping solution. Finally, the proposed ditch line characterization strategies are tested using datasets C-1 and C-2.

Datasets A-1, A-2, and A-3 were collected over a county road, CR500N, in Indiana, USA. An aerial photo of the study site is presented in Figure 3.2a, and an image capturing location PA1 taken by the front left Grasshopper camera on the PWMMS-HA is shown in Figure 3.2b. This study site is located at a densely vegetated hill, as can be seen from the aerial photo. The average slope along the road is 6% (approximately 20 m elevation change over a planimetric distance of 350 m). The roadside ditches are present on both sides of the road and covered by short vegetation. At the time of this data acquisition, the indicated study site was being reworked to change the S-curve of the road to a simple curve with the goal of improving traffic safety. Cut trees

Figure 3.2 Study site at CR500N: (a) the surveyed area and cross-section locations (aerial photo adapted from Google, 2018a) and (b) image of the surveyed area at location PA1 captured by one of the cameras onboard the PWMMS-HA.

TABLE 3.2
The range of standard deviation of the estimated system mounting parameters for all the LiDAR units/cameras onboard each MLMS

	LiDAR Units				
	UAV	**UGV**	**Backpack/Mobile-Pack**	**PWMMS-HA**	**PWMMS-UHA**
Lever Arm	±1.2–1.5 cm	±1.0–1.3 cm	±0.5–0.8 cm	±0.8–1.8 cm	±0.5–0.6 cm
Boresight	±0.02°–0.04°	±0.02°–0.08°	±0.02°–0.03°	±0.02°–0.05°	±0.01°–0.02°
	Camera Units				
	UAV	**UGV**	**Backpack/Mobile-Pack**	**PWMMS-HA**	**PWMMS-UHA**
Lever Arm	±2.7–5.4 cm	±3.7–6.5 cm	±3.0–4.9 cm	±3.8–6.6 cm	±3.1–6.0 cm
Boresight	±0.03°–0.04°	±0.12°–0.14°	±0.08°–0.12°	±0.07°–0.14°	±0.06°–0.11°

TABLE 3.3
Expected accuracy of the ground coordinates evaluated using the LiDAR Error Propagation calculator (Habib et al., 2006)

	UAV	**UGV**	**Backpack/Mobile-Pack**	**PWMMS-HA**	**PWMMS-UHA**
Sensor-to-Object Distance	50 m	5 m	5 m	30 m	30 m
Accuracy	±5–6 cm	±2–4 cm	±2–3 cm	±2–3 cm	±2 cm

TABLE 3.4
Specifications of acquired datasets by the different MLMS units for this study

ID	**Location**	**Data Collection Date**	**System**	**Number of Tracks**	**Average Speed (mph)**	**Data Acquisition Time (min)**	**Length (mile)**
A-1	CR500N	2021/03/13	UAV	4	8	12	0.4
A-2		2021/03/26	PWMMS-HA	2	29	4	0.5
A-3		2021/03/26	Mobile-pack	2	20	4	0.5
B-1	McCormick Rd.	2020/12/22	PWMMS-HA	2	20	10	1.6
B-2	and Cherry Ln.	2020/12/22	PWMMS-UHA	2	20	10	1.6
B-3		2020/12/22	UGV	4	4	30	0.5
B-4		2020/12/22	Backpack	4	3	32	0.5
B-5		2021/03/26	Mobile-pack	2	26	4	1.1
C-1	SR 28	2021/03/26	PWMMS-HA	2	47	37	13.2
C-2		2021/03/26	Mobile-pack	2	50 (WB) 30 (EB)	35	13.2

for the road rework can be seen on the right side in Figure 3.2b. The PWMMS-HA and Mobile-pack drove along the road in both directions. The UAV was flown in four tracks over the study site with a flying height of 50 m above ground and a lateral distance of 14 m between neighboring flight lines.

Datasets B-1 to B-5 were collected at the intersection of McCormick Road and Cherry Lane adjacent to Purdue University's campus in West Lafayette, Indiana, USA. The roadside ditches are present on both sides of the road and are covered by short vegetation. The width of these ditches ranges from 2 m to 10 m, and their depth ranges from 0.2 m to 1 m. Figure 3.3 shows an aerial photo of the study site and an image capturing location PB3 taken by the front left Grasshopper camera on the PWMMS-HA. To evaluate the absolute accuracy of the LiDAR-based mapping of the ditches, an RTK-GNSS survey was carried out at four cross-section locations—PB1, PB2, PB3, and PB4 in Figure 3.3a. For each profile, the team surveyed few points on the road and 20 to 25 points across the ditch. The team also took few measurements on the sidewalk that was adjacent to the road in profiles PB3 and PB4. The PWMMS-HA, PWMMS-UHA, UGV, and Backpack data were acquired on the same date when the RTK-GNSS survey was conducted. The PWMMS-HA and PWMMS-UHA covered all routes in both directions, so both datasets have two tracks. In contrast to the wheel-based systems, the UGV and Backpack acquired data along the ditches on both sides of the road in forward and backward directions, resulting in four tracks over the surveyed area. The Mobile-pack data was acquired at a later date (approximately three months from the RTK-GNSS and other MLMS units surveys, refer to Table 3.4). The system

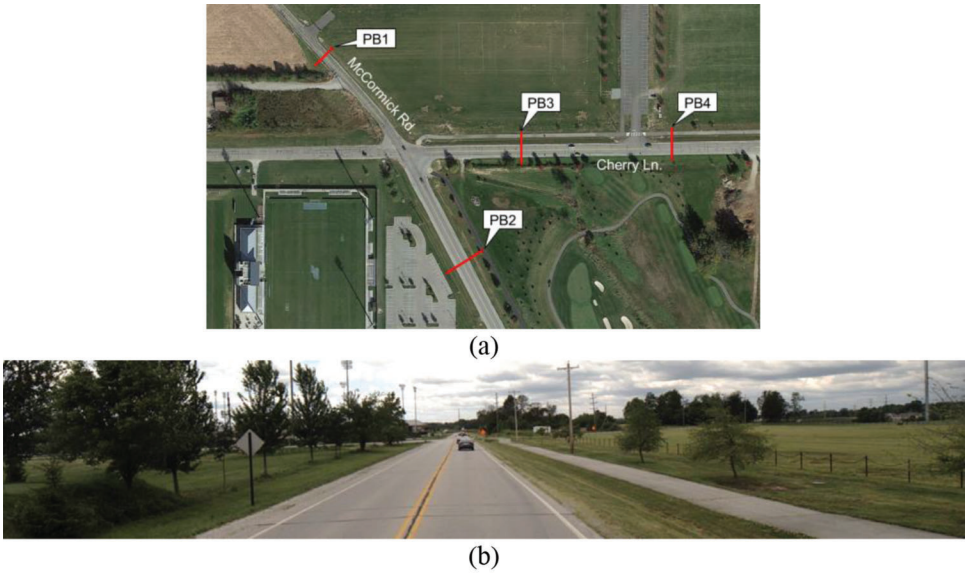

Figure 3.3 Study site at McCormick Rd: (a) surveyed area and cross-section locations (aerial photo adapted from Google, 2018b), and (b) image of the surveyed area at location PB3 captured by one of the cameras onboard the PWMMS-HA.

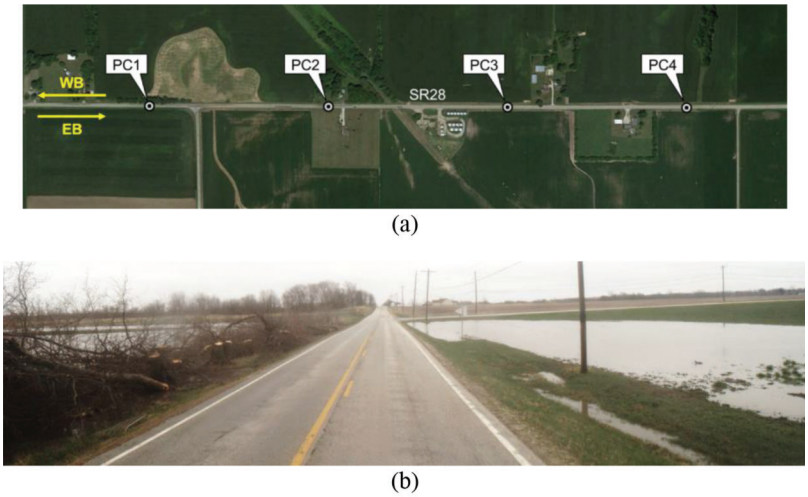

Figure 3.4 Study site at SR 28: (a) the one-mile-long region of interest and cross-section locations (aerial photo adapted from Google, 2018c) and (b) image of the surveyed area at location PC1 captured by one of the cameras onboard the PWMMS-HA.

drove along Cherry Lane and the south part of McCormick Road in both directions. Location PB1 was not covered in this survey.

Datasets C-1 and C-2 were collected over a state road, SR 28, in Indiana, USA with a total length of approximately 13 miles. The roadside ditches are present on both sides of the road and are covered by short vegetation and shrubs. A one-mile-long segment was selected as the region of interest. Figure 3.4a shows an aerial photo of the ROI where PC1, PC2, PC3, and PC4 are four cross-section locations that are used in the ditch line characterization analysis (as will be discussed later in Section 5.3). Figure 3.4b is an image capturing location PC1 taken by the front left Grasshopper camera on the PWMMS-HA. As can be seen in the image, some parts of the ditches and adjacent agricultural fields were flooded. Also seen is some cut-down trees for an upcoming road maintenance project. Both PWMMS-HA and Mobile-pack drove westbound and eastbound on SR 28, and therefore both datasets have two tracks. The PWMMS-HA drove at an average speed of 47 mph in both directions. The Mobile-pack drove at a higher speed (50 mph) in westbound and a lower speed (30 mph) in eastbound. This drive-run configuration was designed for investigating the impact of driving speed on point density as well as to evaluate the system's ability of mapping roadside ditches.

4. METHODOLOGY FOR DITCH MAPPING AND CHARACTERIZATION

The proposed framework for roadside ditch mapping is illustrated in Figure 4.1. The main steps include: (1) ground filtering; (2) point cloud vertical accuracy assessment; (3) cross-sectional profile extraction, visualization, and slope evaluation; (4) drainage network and longitudinal profile extraction; and (5) potential flooded region detection and visualization.

4.1 Ground Filtering and Digital Terrain Model (DTM) Generation

Ground filtering algorithms separate bare earth points (which represent the terrain) from above-ground points and subsequently, generate a rasterized digital terrain model. The bare earth point cloud is a subset of the original point cloud, and thus retains the precision of the latter. The DTM, on the other hand, is a rasterized dataset with decreased precision, which serves as an input for hydrological analyses. In this study, the ground filtering technique is adapted from the cloth simulation algorithm proposed by Zhang et al. (2016). The conceptual basis of the cloth simulation approach can be summarized in four steps: (1) turn the point cloud upside down, (2) define a cloth (consisting of particles and their interconnections) with some rigidness, and place it above the point cloud, (3) let the cloth drop under the influence of gravity to designate the final shape of the cloth as the DTM, and (4) use the DTM to filter ground from above-ground points. In the original approach introduced by Zhang et al. (2016), the rigidness of the cloth is constant, and its value is selected based on the properties of the terrain (i.e., whether the terrain has a gentle slope, terraced slope, or steep slope). This approach was developed for airborne LiDAR, and it does not consider large variation in point density, which is not the case for mobile LiDAR data where the point density decreases as we move away from the road surface. The modified approach deals with this problem by redefining the rigidness of each particle on the cloth based on the point density of an initial bare earth point cloud. The approach consists of three steps: (1) using the original approach to extract the bare earth point cloud, (2) redefining the rigidness of the cloth based on the point density of the bare earth point cloud, and (3) applying the cloth simulation again to obtain a refined bare earth point cloud and the final DTM.

An example of a DTM generated based on the original and modified approaches is shown in Figure 4.2. In the area shown in Figure 4.2a, the point cloud is dense along the road surface but is sparse within the grass areas, especially on the right side of the road where there are no points in some areas. The original approach leads to artifacts in low point density areas as the cloth keeps dropping without being stopped by the ground. By manipulating the rigidness of the cloth depending on the point density within the neighborhood, the modified approach is able to generate a reasonable representation of the terrain, even if there are gaps in the point cloud. The difference between the resultant DTM from the two approaches is visualized by generating an elevation difference map, as in Figure 4.2a. Areas with low point density are observed to be largely impacted by the difference in the two approaches with artifacts extending to an elevation difference at the range of 1.5 m. The side view of a cross-sectional profile across the road is illustrated in Figure 4.2b to highlight the obvious difference in the DTM portion on the right side due to sparse points. In general, the derived DTM from the modified approach traces the terrain well (see Figure 4.2c).

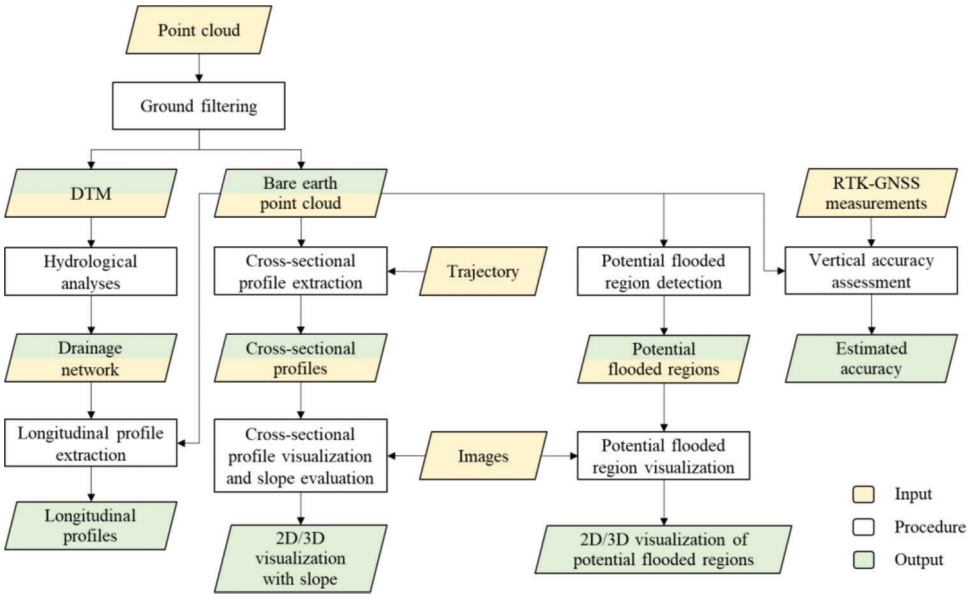

Figure 4.1 Main steps of the proposed framework for point cloud quality assessment and ditch mapping/characterization.

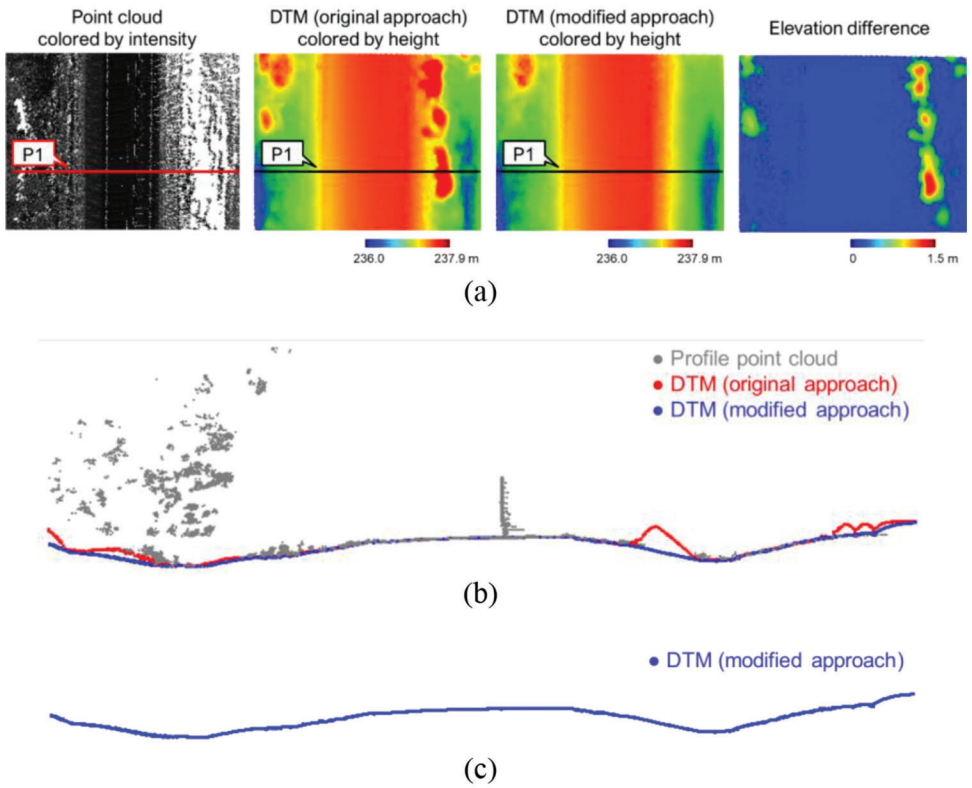

Figure 4.2 Comparison between the original and modified approaches for DTM generation: (a) point cloud, DTM based on original and modified approaches and elevation difference between the two DTMs, (b) side view of profile P1 showing point cloud, DTM based on original and modified approaches, and (c) side view of profile P1 showing only DTM based on the modified approach.

4.2 Point Cloud Quality Assessment

Quality assessment involves evaluating the (1) relative accuracy: alignment between point clouds from different MLMS units, and (2) absolute accuracy: agreement between the point cloud and independently measured ground control points.

The assessment of relative accuracy between two point clouds quantifies the degree of consistency among conjugate points/features. Applying the approach proposed by Lin and Habib (2021), the net discrepancy between two point clouds is estimated using planar features—terrain patches—extracted from the acquired data. Starting with two bare earth point clouds from different MLMS units, one is selected as a reference and another as a source. The bare earth point clouds are then segmented into patches with a pre-determined size. For each patch, a principal component analysis (PCA) is performed to test its planarity, as proposed by Habib and Lin (2016). Only planar patches are included in subsequent analysis. An iterative plane fitting is then carried out to remove potential outlier points and estimate the parameters of the plane. A patch is rejected from the accuracy assessment if: (1) the plane-fitting Root Mean Square Error (RMSE) exceeds a user-defined threshold, or (2) the remaining points after iterative plane fitting fails to reach another user-defined threshold. Next, the center of the reference plane (a_i) and its projection on the source plane (b_i) are determined. The discrepancy between conjugate patches, $[d_{x\_obs}\ d_{y\_obs}\ d_{z\_obs}]^T$ can therefore be quantified by the coordinate difference between a_i and b_i (as depicted in Figure 4.3).

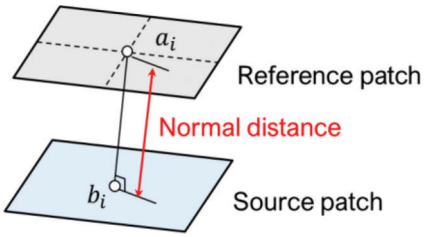

Figure 4.3 Illustration of the discrepancy estimation using conjugate terrain patches.

The net discrepancy between two point clouds is estimated using a least squares adjustment (LSA). For feature-based pairing, each planar feature provides discrepancy information only along the normal direction to the plane. The inability to estimate the discrepancy along planar features is considered within the LSA model by incorporating a modified weight matrix (Ravi, in press; Renaudin et al., 2011). The modified weight matrix is derived such that it retains only the component of the discrepancy along the normal direction to the planar feature in question. The LSA

model with modified weight matrix estimates the X, Y, and Z shifts between two point clouds using the mathematical model in Equation 4.1). The discrepancies between conjugate terrain patches ($[d_{x\_obs}\ d_{y\_obs}\ d_{z\_obs}]^T$) are direct observations of the net discrepancy between two point clouds ($[d_x\ d_y\ d_z]^T$). The random noise $[e_x\ e_y\ e_z]^T$ has a mean of zero and variance-covariance matrix of $\sigma_0^2 P'^{+}_{xyz}$, with σ_0^2 is the a-priori variance factor and P'_{xyz} is the modified weight matrix. The plus sign denotes the Moore–Penrose pseudoinverse since P'_{xyz} is rank-deficient and its inverse does not exist. One should note that although the least squares adjustment evaluates the discrepancies along the X, Y, and Z directions, the reliability of these estimates depends on the variation in the orientation/slope/aspect within the region of interest. For transportation corridors, the terrain patches are mostly flat or have a mild slope, and thus provide discrepancy information mainly along the vertical direction. Therefore, only the vertical discrepancy estimation is reported.

$$\begin{bmatrix} d_{x\_obs} \\ d_{y\_obs} \\ d_{z\_obs} \end{bmatrix} = \begin{bmatrix} d_x \\ d_y \\ d_z \end{bmatrix} + \begin{bmatrix} e_x \\ e_y \\ e_z \end{bmatrix},\ e \sim \left(0, \sigma_0^2 P'^{+}_{xyz}\right) \qquad \text{(Eq. 4.1)}$$

The absolute accuracy is assessed against manually collected RTK-GNSS measurements (hereafter, RTK points). To investigate the LiDAR mapping accuracy over different surfaces, we manually classify the LiDAR/RTK points into two classes: solid surface (including road and sidewalk) and vegetated area. The elevation difference between each RTK point and its closest LiDAR point is calculated and the RMSE and interquartile range are reported for each class.

4.3 Cross-Sectional Profile Extraction, Visualization, and Slope Evaluation

A cross-sectional profile with a given length and width can be extracted from the point cloud, bare earth point cloud, and/or DTM at any location. The orientation of the profile should be perpendicular to the direction of the road, which can be derived using the vehicle trajectory information. Once the profile is extracted, the slope along the profile is evaluated using the bare earth points, a sample result is shown in Figure 4.4. The profile and slope information extracted from LiDAR data can then be compared to the design/standard values (McGee et al., 2009) to detect problems such as improper grade. Furthermore, using the trajectory information, it is possible to crop and analyze a series of cross-sectional profiles automatically based on a user-defined interval.

The key strength of mobile mapping systems lies in the integration of information acquired from different sensors onboard the system. Since all the sensors' data is georeferenced to a common reference frame, multi-sensor/multi-date datasets can be effectively fused. That is, the images capturing each profile can be identified, and the profile can be back-projected to the images. Consequently, the ditches can be visualized in both 3D point clouds and 2D images even though they are mainly detected and mapped in 3D space. The image-based visualization is useful for effective mitigation of detected problems during ditch mapping (e.g., deviation from the design profile of the ditch, improper grade, and/or debris within the ditch).

4.4 Drainage Network and Longitudinal Profile Extraction

Conducting a drainage network analysis is critical because it signifies the location of valley points along the ditches and it also identifies potential drainage issues. The drainage network through which water travels can be identified by analyzing the movement of surface water—that is, calculating the flow direction and flow accumulation for each DTM cell (Jenson & Domingue, 1988). When enough water flows through a cell, the location is considered to have a stream passing through it. Therefore, the drainage network can be extracted by applying a user-defined threshold on the flow accumulation map. The major streams are expected to be aligned with the "valley" of the ditches (Figure 4.5). Combining the resulting drainage network with other information derived from MLMS can facilitate long-term road and pavement management. For instance, by overlapping the drainage network with detected lane markings (which specifies the boundaries of the road) as well as detected potholes, one can identify potential road flooding areas if there is high flow accumulation on the road. The drainage network can also be used to investigate the possibility of correlating ditch adequacy to pavement performance, for example, pavement distress caused by drainage problems.

A longitudinal profile is the one along the "valley" of a ditch; that is, it aligns with the major stream in the drainage network. Figure 4.6a shows an example of the

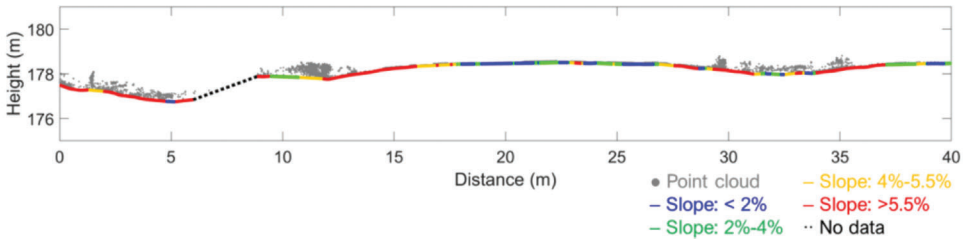

Figure 4.4 An example of cross-sectional profile colored by slope.

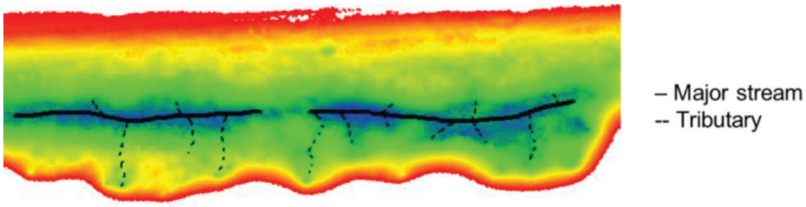

Figure 4.5 Sample drainage network of a roadside ditch showing a major stream and its tributaries.

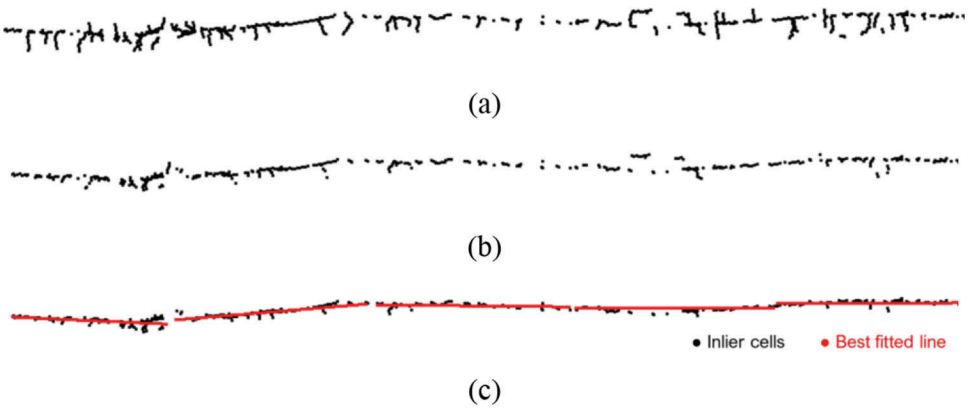

Figure 4.6 Longitudinal profile extraction: (a) drainage network, (b) drainage network after removing tributaries, and (c) streamlines after outlier removal.

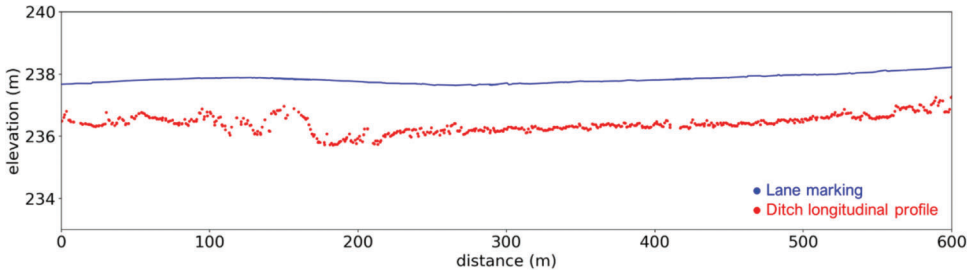

Figure 4.7 An example of a longitudinal profile together with the detected lane marking.

drainage network extracted from MLMS data, from which some tributaries and discontinuities along the major streams can be observed. To identify the location of the longitudinal profile, we need to remove tributaries and connect major streams. Since our focus is the ditches adjacent to a transportation corridor, the drainage network is expected to be a long, linear feature. Line fitting is performed to estimate the line parameters, which, in turn, are used to find the direction of the major stream. The drainage network is then rotated so that the direction of the major stream is along the X-direction. The tributaries are removed based on the assumption that within a small range of the X-coordinate of the rotated drainage network, the elevation of the major stream is lower than the elevation of the tributaries. A sample result is shown in Figure 4.6b. Next, we divide the streamlines into segments and apply line fitting and outlier removal using a random sample consensus (RANSAC) strategy (Fischler & Bolles, 1981), depicted in Figure 4.6c, assuming that the ditch line is approximately a straight line within each segment. The longitudinal profile is extracted based on the location of the inlier streamlines and best-fitted lines. Figure 4.7 illustrates a sample longitudinal profile, together with the detected lane marking that signifies the elevation of the road surface. The longitudinal profile of a ditch is the primary information for analyzing flood risk. Sudden elevation changes along the longitudinal profile can serve as an indication of potential problems including improper grade along the ditch or debris within the ditch. This can be further confirmed by inspecting the images that capture the area.

4.5 Potential Flooded Region Detection and Visualization

Standing water is an indication of drainage issues/high flooding risk. Therefore, the ability to identify such areas is critical for prioritizing and planning maintenance. The proposed flooded region detection approach is based on the hypothesis that LiDAR has zero return over water bodies. Potential flooded regions

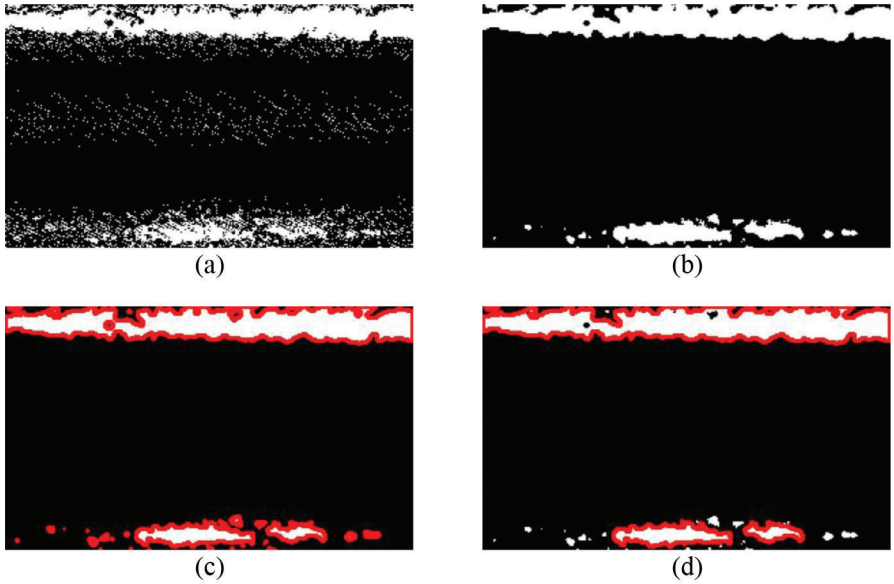

Figure 4.8 Water detection approach: (a) binary point density image, (b) image after applying median filter, (c) boundary tracing result, and (d) detected water areas after removing small regions.

Figure 4.9 An example of a potential flooded region visualized in (a) 3D point cloud and (b) 2D image.

can be identified by detecting areas where the LiDAR points are absent. The approach has four steps, as illustrated in Figure 4.8. First, a binary point density image over the region of interest is generated with a user-defined cell size where 0 means there are at least one point in the cell and 1 means there is no point in the cell. A median filter is then applied to reduce the noise caused by irregular point distribution. Next, the boundary between the black and white cells is traced using an OpenCV implementation of the algorithm proposed by Suzuki and Be (1985). An ROI is reported if its area is larger than a user-defined threshold. With the ability of 2D–3D cross-visualization, the reported ROIs are visualized both in 3D point cloud and 2D images. A sample result is shown in Figure 4.9. The image-based visualization helps to identify false detection, and it also helps to associate any environmental factors that lead to flooding.

The potential flooded region detection results are compared against manually established ground truth. The manual flooded region identification is carried out by examining the point cloud and images captured by the PWMMS-HA over the ROI and manually marking all the flooded regions. To evaluate the performance of the proposed potential flooded region detection strategy, precision and recall—as represented by Equations 4.2 and 4.3 where TP, FP, and FN are the true positives, false positives, and false negatives, respectively—are used. Precision signifies how accurate the positive predictions are whereas recall indicates how well the true flooded regions are identified.

$$Precision = \frac{TP}{TP + FP} \qquad \text{(Eq. 4.2)}$$

$$Recall = \frac{TP}{TP + FN} \qquad \text{(Eq. 4.3)}$$

5. EXPERIMENTAL RESULTS AND DISCUSSION

In this section, we present three experimental results. The first experiment compares the ground-based systems against UAV in terms of the ability of mapping roadside ditches. The second experiment evaluates the comparative performance of different grades of MLMS

and identifies the most feasible technique for ditch mapping. The third experiment tests the proposed ditch line characterization approach using a one-mile-segment along a state road.

5.1 Comparison Between Ground-Based and UAV Systems for Mapping Roadside Ditches

In this section, the capability of ground-based MLMS for monitoring roadside ditches is assessed against a UAV-based MLMS. Datasets A-1 (captured by the UAV), A-2 (captured by the PWMMS-HA), and A-3 (captured by the Mobile-pack) were used for this analysis. The ground-based MLMS mapping products were compared against those from the UAV in terms of the spatial coverage, point density, and relative vertical accuracy between point clouds.

The point cloud and bare earth point cloud were first generated from each dataset. Figure 5.1a shows the point clouds from different MLMS units together with the trajectory. While the ground-based MLMS units can only drive on road and therefore the point cloud coverage is limited to areas adjacent to the road, theoretically, there is no such limitation on the flight movement for the UAV. For the datasets used in the current analysis, the UAV was able to maneuver over a large area and obtain a wide spatial coverage. The bare earth point clouds were extracted using the modified cloth simulation approach and the results are depicted in Figure 5.1b. A cross-sectional profile at location PA1 was extracted from the original and bare earth point clouds. The profile side view, as shown in Figure 5.2, demonstrates that the LiDAR points were able to penetrate the vegetation and capture the terrain. Compared to the UAV, the ground-based systems are more prone to occlusions caused by terrain features. Having said that, all three systems show complete coverage over the road surface and ditches, which are the focus of this study.

The point density map for each dataset was derived based on the bare earth point cloud since the latter is the one used for ditch line characterization. Figure 5.3 shows the point density maps along with the trajectory for the UAV, PWMMS-HA, and Mobile-pack. The statistics of point density, including the 25th percentile, median, and 75th percentile in the surveyed area, are reported in Table 5.1. The ground-based systems produced much higher point density as compared to the UAV due to the short sensor-to-object distance. PWMMS-HA had the highest point density since its point cloud came from four LiDAR units. Looking into the spatial pattern in Figure 5.3, the point density from the ground-based systems is high near the trajectory, and it decreases drastically as the distance from the trajectory increases. Such spatial pattern is mainly related to the varying sensor-to-object distance and occlusion caused by trees. For the UAV, in contrast, the sensor-to-object distance (i.e., flying height) was almost constant throughout the data collection, and thus the variation in point density across the surveyed area is much smaller.

The relative vertical discrepancies between point clouds from different systems were estimated using the terrain patches extracted from the bare earth point clouds. The size of the terrain patches was set to 0.5 m × 0.5 m. The square root of a-posteriori variance factor ($\widehat{\sigma_0}$) and the estimated vertical discrepancy (d_z) between the point clouds from different MLMS units

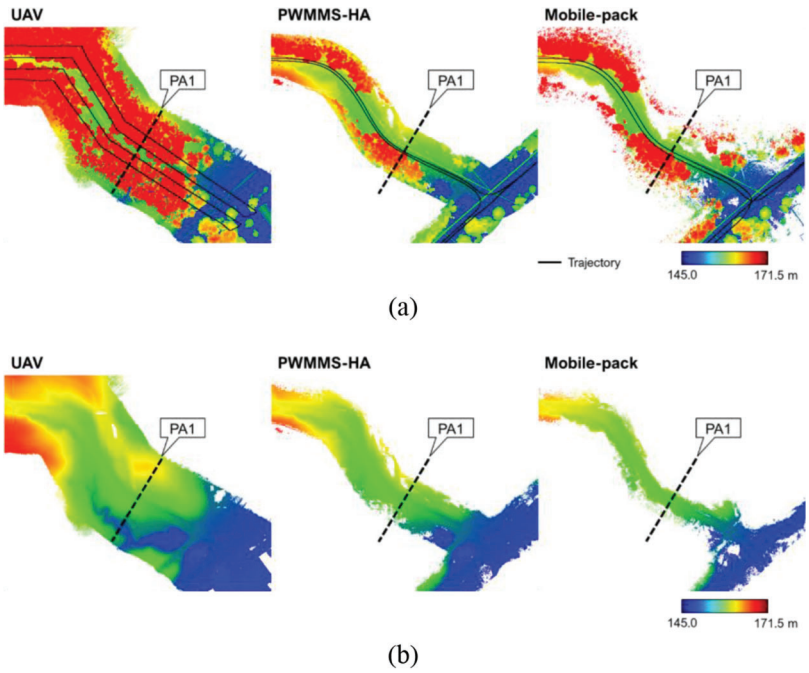

Figure 5.1 MLMS mapping products showing the (a) point cloud and trajectory and (b) bare earth point cloud from UAV, PWMMS-HA, and Mobile-pack.

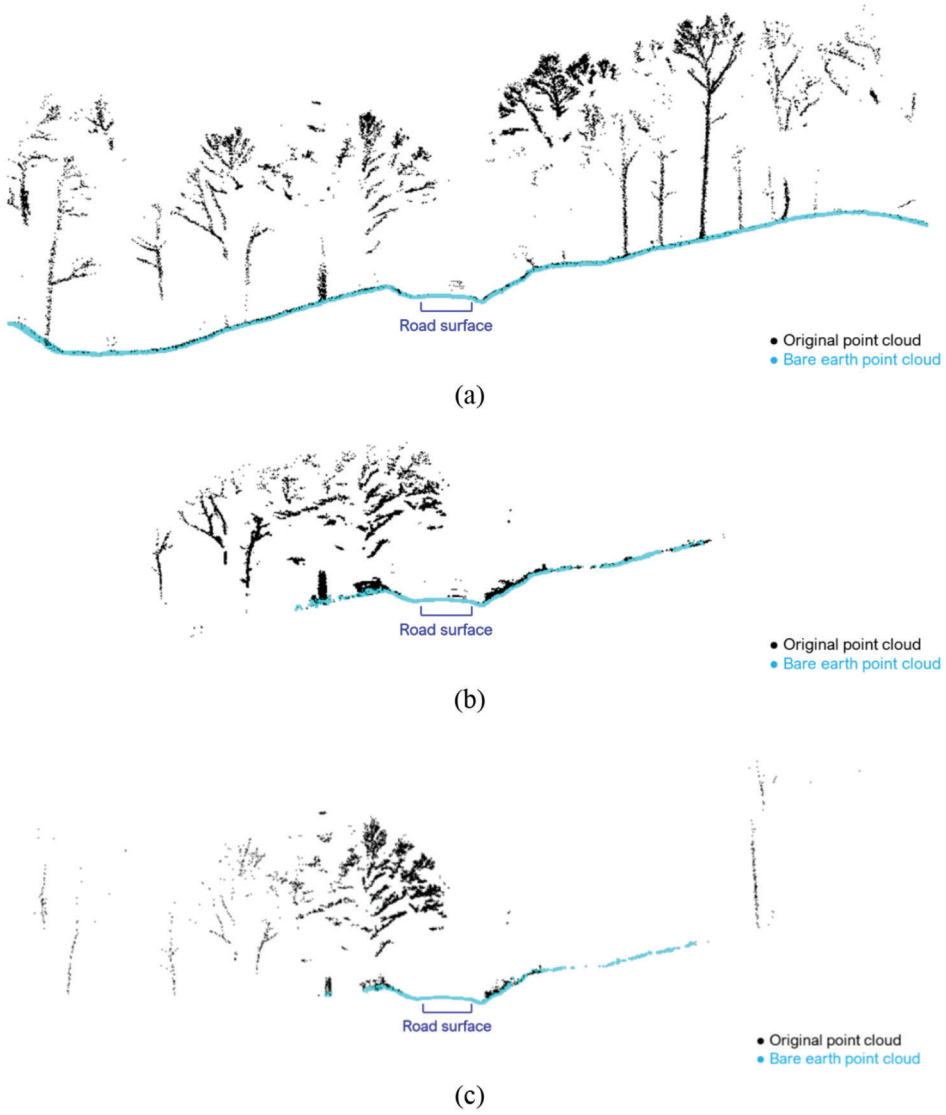

Figure 5.2 Side view of a cross-sectional profile at location PA1 showing the original and bare earth point clouds from (a) UAV, (b) PWMMS-HA, and (c) Mobile-pack.

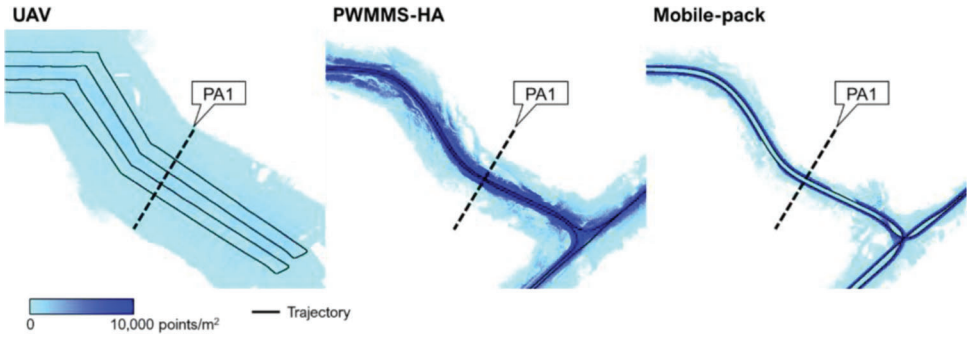

Figure 5.3 Point density of the bare earth point cloud along with the trajectory from UAV, PWMMS-HA, and Mobile-pack.

are reported in Table 5.2. The former reflects the noise level of the point clouds, and the latter signifies the overall net discrepancy between the point clouds in question. As mentioned earlier, the ability to estimate the discrepancies along the X, Y, and Z directions relies on the variation in the orientation/slope/aspect within the region of interest. In this study site, the relatively horizontal terrain cannot provide sufficient information for estimating planimetric discrepancies. Therefore, only the vertical discrepancy estimation is reported.

TABLE 5.1
Statistics of the point density in the surveyed area

Dataset	Point Density (points/m^2)		
	25th Percentile	Median	75th Percentile
A-1 (UAV)	200	500	1,000
A-2 (PWMMS-HA)	500	1,800	6,100
A-3 (Mobile-pack)	400	1,200	3,800

TABLE 5.2
Estimated vertical discrepancy and square root of a-posteriori variance using A-1 (UAV), A-2 (PWMMS-HA), and A-3 (Mobile-pack) datasets

Reference	Source	Number of Observations	$\widehat{\sigma_0}$ (m)	d_z (m)	
				Parameter	Std. Dev.
UAV	PWMMS-HA	111,973	0.083	0.028	2.615×10^{-4}
UAV	Mobile-pack	55,742	0.064	-0.008	2.864×10^{-4}
PWMMS-HA	Mobile-pack	67,133	0.043	-0.029	1.671×10^{-4}

According to Table 5.2, the square root of a-posteriori variance factor suggests a noise level of ± 4–8 cm. The discrepancy estimation shows that all datasets are in agreement within a ± 3 cm range along the vertical direction.

The discussion above reveals that all the MLMS units can achieve similar mapping accuracy. The advantage of UAV is that it can maneuver over areas that are difficult to reach by ground-based vehicles. However, UAV surveys can only cover a relatively small area due to the limited flying speed, battery life, and maintaining line-of-sight regulations. Thus, it is not a practical solution for mapping long, linear transportation corridors. Field surveys with ground-based MLMS units, on the other hand, are more efficient since the vehicles can travel at a higher speed and cover a longer extent. As long as the region of interest is limited to areas adjacent to the road, MLMS data can have full coverage with a decent point density, which is adequate for monitoring roadside ditches.

5.2 Comparative Performance of Different Ground-Based MLMS Units

In this experiment, the ability of different ground-based MLMS units for mapping roadside ditches was evaluated. Datasets B-1 (captured by the PWMMS-HA), B-2 (captured by the PWMMS-UHA), B-3 (captured by the UGV), B-4 (captured by the Backpack), and B-5 (captured by the Mobile-pack) were used in this analysis. The comparative performance of different MLMS units was assessed in terms of spatial coverage, relative vertical accuracy, and absolute vertical accuracy.

Upon reconstructing the point cloud, the bare earth point cloud was extracted, and the DTM was generated using the modified cloth simulation approach for each dataset. Cross-sectional profiles at locations PB1, PB2, PB3, and PB4 were extracted from the point cloud, bare earth point cloud, and DTM with a width of 1 m. Figure 5.4 shows the cross-sectional profiles of the bare earth point clouds from different MLMS units at location PB3. The spatial coverage of point clouds from different systems was evaluated qualitatively. As can be observed in Figure 5.4, with sufficient number of tracks, each of the mobile mapping systems demonstrates a complete coverage of the ditch. The UGV point cloud, despite having full coverage over the ditches, has limited coverage of the road and areas that are away from the tracks. For the UGV, the location of tracks with respect to the ditch plays a crucial role. Since the UGV tends to be very close to the ground, it is prone to occlusions caused by surrounding vegetation and terrain. The Mobile-pack has the least number of points because it has only one LiDAR unit covering two tracks over the region of interest, and the vehicle to which the sensor assembly was mounted traveled at a speed similar to those of the PWMMS-HA and PWMMS-UHA. One thing to note is that the point density of Mobile-pack drops rapidly when moving away from the trajectory. This is attributed to the mounting orientation of its LiDAR sensor whose field of view was limited to focus on objects in short range (refer to Figure 3.1d and the discussion in Section 3.1).

The relative vertical accuracy between point clouds from different MLMS units was evaluated using planar features—terrain patches—extracted from the bare earth point clouds over the surveyed area. The size of the terrain patches was set to 0.5 m $\times$ 0.5 m. The PWMMS-HA dataset was selected as a reference because it had the largest spatial coverage. Table 5.3 reports the square root of a-posteriori variance factor ($\widehat{\sigma_0}$) and estimated vertical discrepancy (d_z) between the point clouds from different MLMS units. The square root of a-posteriori variance factor suggests a noise level of ± 1–2 cm. The point clouds from different

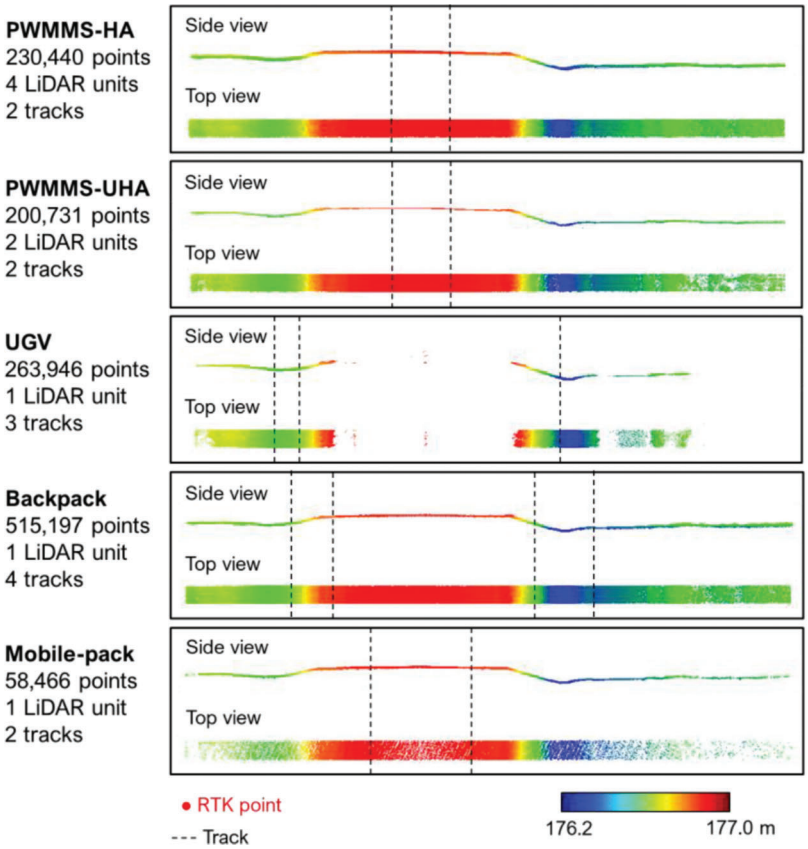

Figure 5.4 Cross-sectional profiles at location PB3 from different systems showing the side view, top view, and the platform tracks (black dashed lines).

TABLE 5.3
Estimated vertical discrepancy and square root of a-posteriori variance using B-1 (PWMMS-HA), B-2 (PWMMS-UHA), B-3 (UGV), B-4 (Backpack), and B-5 (Mobile-pack) datasets

				d_z (m)	
Reference	**Source**	**Number of Observations**	$\hat{\sigma_0}$ **(m)**	**Parameter**	**Std. Dev.**
PWMMS-HA	PWMMS-UHA	13,610	0.010	-0.013	8.711×10^{-5}
PWMMS-HA	UGV	4,737	0.021	0.007	3.385×10^{-4}
PWMMS-HA	Backpack	12,480	0.012	-0.027	1.137×10^{-4}
PWMMS-HA	Mobile-pack	11,539	0.018	-0.019	1.750×10^{-4}

MLMS units exhibit a good degree of agreement with an overall precision of ± 1–3 cm.

The absolute accuracy of the point cloud from different MLMS units was assessed against the RTK-GNSS survey. Figure 5.5 shows the side view of the RTK points together with the bare earth point cloud and DTM from each MLMS at location PB3. Through visual inspection, one can see that the DTMs trace the terrain well and are in good agreement with the RTK points along the vertical direction. As mentioned in Section 4.2, the LiDAR/RTK points are classified into two classes: solid surface (including road and sidewalk) and vegetated area. The elevation difference between each RTK point and its closest LiDAR point is calculated, and the interquartile range is visualized, as shown in Figure 5.6. The variance of elevation differences is small for solid surfaces and large for vegetated areas. The vertical accuracy was found to be ± 1 cm (PWMMS-HA), ± 1 cm (PWMMS-UHA), ± 2 cm (UGV), ± 1 cm (Backpack), and ± 2 cm (Mobile-pack) for solid surfaces. For areas with vegetation, the vertical accuracy was found to be ± 5 cm, ± 7 cm, ± 7 cm, ± 4 cm, and ± 7 cm for PWMMS-HA, PWMMS-UHA, UGV, Backpack, and Mobile-pack, respectively. The PWMMS-HA and Backpack, despite with cm-level accuracy LiDAR units, had a slightly better performance mainly attributed to better penetration of vegetated surfaces due to their higher point density and larger beam divergence angle of the Velodyne units.

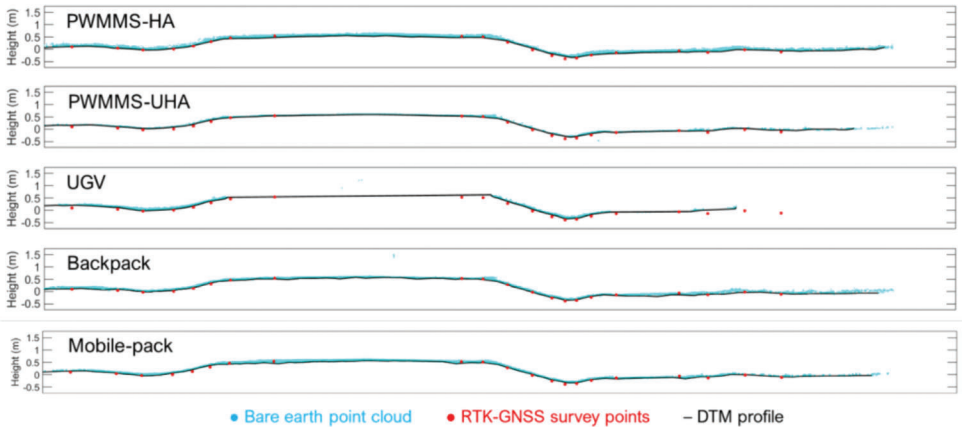

Figure 5.5 Cross-sectional profile at location PB3 showing the point cloud, DTM, and RTK-GNSS survey points.

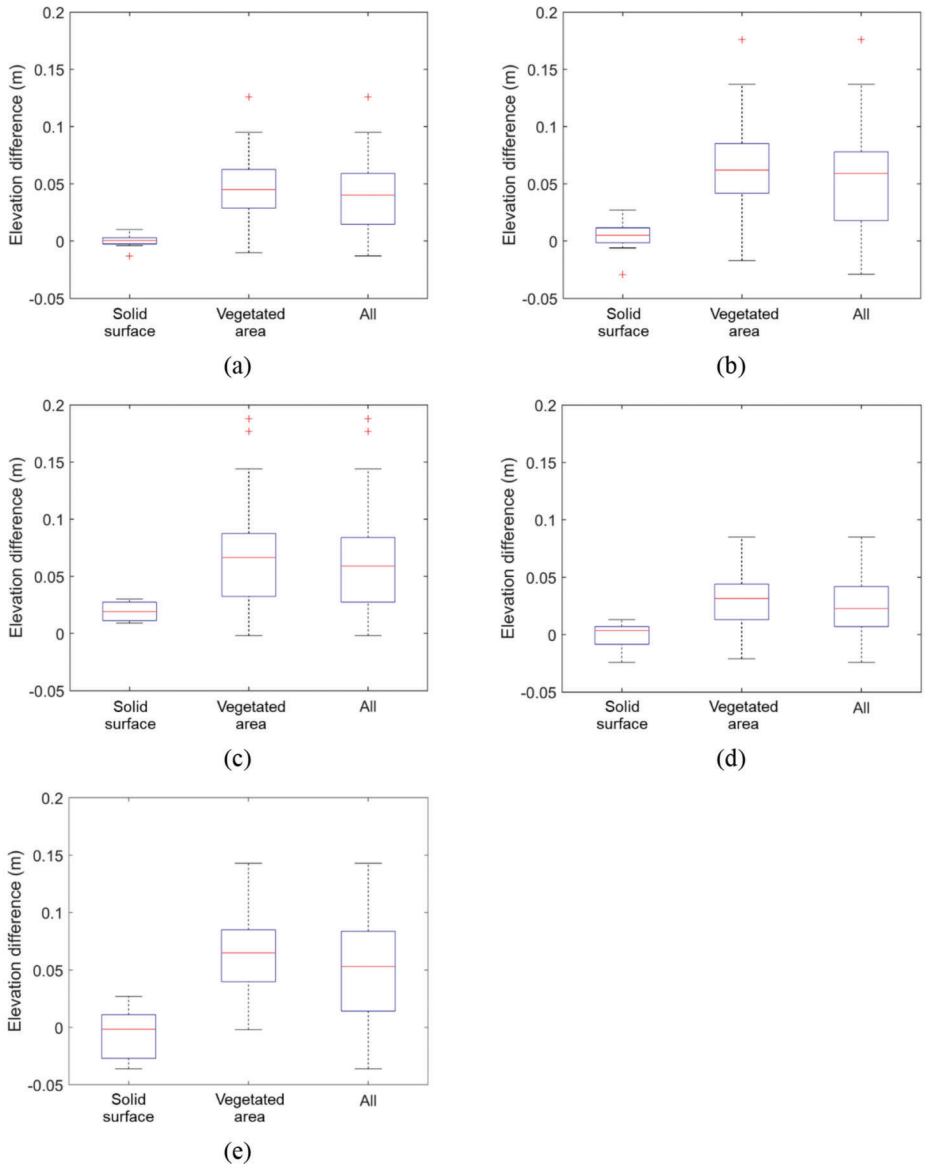

Figure 5.6 Statistics of elevation difference between RTK-GNSS surveyed points and LiDAR points for (a) PWMMS-HA, (b) PWMMS-UHA, (c) UGV, (d) Backpack, and (e) Mobile-pack with residual plots of range, 25th percentile, median, and 75th percentile.

In this section, the spatial coverage, relative vertical accuracy, and absolute vertical accuracy of point clouds from five ground-based MLMS units were evaluated. The results suggest that all the MLMS units can have a complete coverage of the roadside ditches with sufficient number of tracks. UGV is less desirable because it is prone to occlusions. The ditch mapping accuracy of different MLMS units was found to be similar. Systems with high-end LiDAR units are not necessarily better for mapping roadside ditches. In terms of field survey, UGV, and Backpack are not practical for mapping long extent of transportation corridors. Consequently, the PWMMS-HA and Mobile-pack are practical solutions for mapping roadside drainage ditches.

5.3 Ditch Line Characterization Using LiDAR Data

The previous section concluded that the PWMMS-HA and Mobile-pack are more appropriate for capturing roadside ditches. In this experiment, the proposed ditch line characterization was tested using data acquired by the two systems: datasets C-1 (collected by PWMMS-HA) and C-2 (collected by Mobile-pack). The results for the one-mile-long region of interest are presented in this section, showing the following.

- Bare earth point cloud and corresponding DTM.
- Cross-sectional profiles in 3D and 2D, together with the slope evaluation results.
- Drainage network and longitudinal profiles.
- Potentially flooded areas.

Upon reconstructing the point cloud, the bare earth point cloud and DTM were generated for each MLMS dataset using the modified cloth simulation approach, and the corresponding point density map was derived based on the bare earth point cloud. Figure 5.7 show the point cloud (with trajectory), bare earth point cloud, DTM, and point density map (with trajectory) from PWMMS-HA and Mobile-pack over an area covering location PC2 (see Figure 3.4). The bare earth point cloud is a subset of the point cloud, and therefore a non-uniform distribution of the points can be observed (see Figure 5.7b). The DTM is a rasterized dataset and therefore has a uniform distribution within

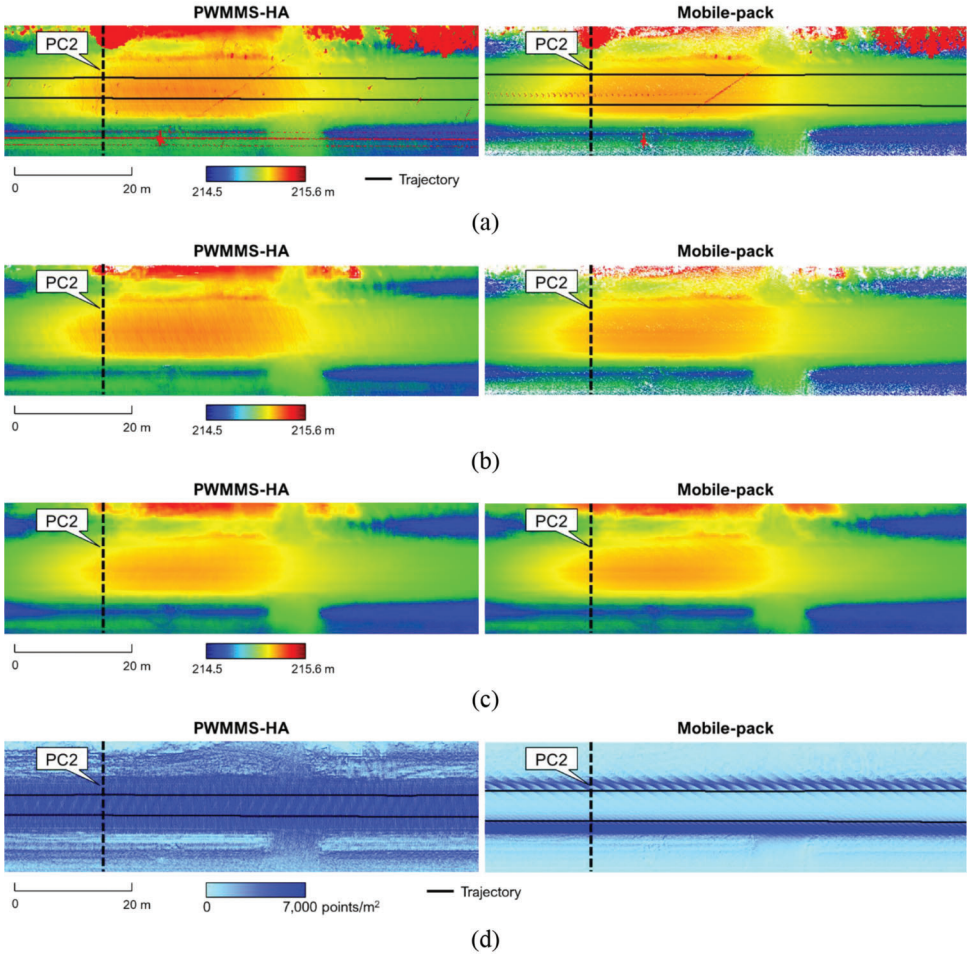

Figure 5.7 LiDAR-based products from PWMMS-HA and Mobile-pack (showing an 80-meter- long area near location PC2): (a) point cloud and trajectory, (b) bare earth point cloud, (c) digital terrain model (DTM), and (d) point density of the bare earth point cloud and trajectory.

the ROI. In Figure 5.7c, the DTM based on the modified cloth simulation approach captures the terrain even though there are some gaps in the point cloud. Prior to ditch line characterization, we inspected the point density of the bare earth point cloud (Figure 5.7d) from the two MLMS units. For both systems, the point density decreased as the distance from the trajectory increases. The degradation in point density for Mobile-pack is much larger than that of the PWMMS-HA. This is mainly related to the LiDAR unit orientation on the platforms, as we noted earlier. As shown in Figure 5.7d, PWMMS-HA has a decent point density up to 20 m to the left and right of the road edge. Mobile-pack, on the other hand, mainly covers an area within 6 m from the road edge. In this study site, the roadside ditches are typically present within 5 m from the road edge. Therefore, both systems have full coverage over the ditches for subsequent analysis. Another pattern that can be observed from the Mobile-pack point density map is the consistently lower point density along the westbound as compared to the eastbound. This is a result of the different driving speeds—50 mph in westbound and 30 mph in eastbound.

Cross-sectional profiles at locations PC1, PC2, PC3, and PC4 were extracted and the slope along each profile was calculated. Sample results showing profile PC2 are visualized in Figure 5.8. The profile side view shown in Figure 5.8a demonstrates that the LiDAR points were

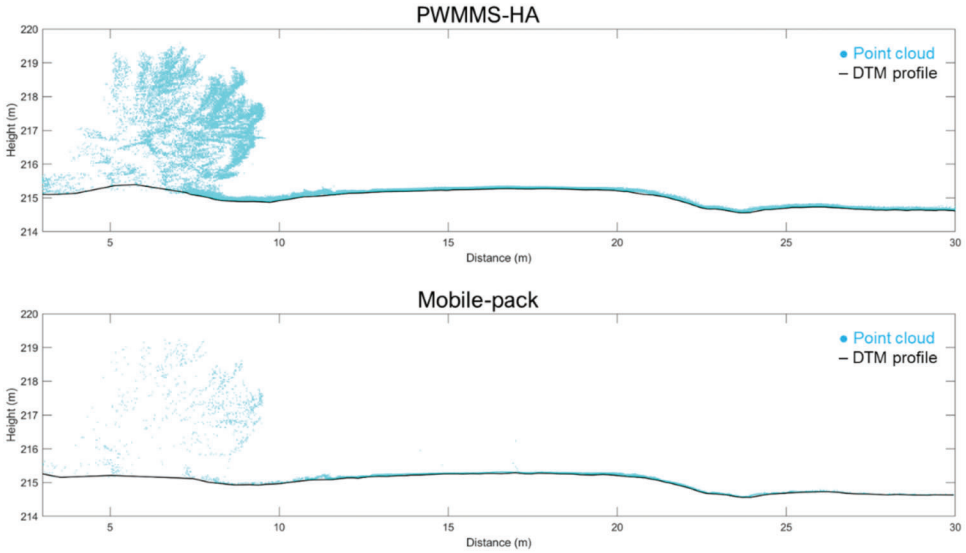

(a)

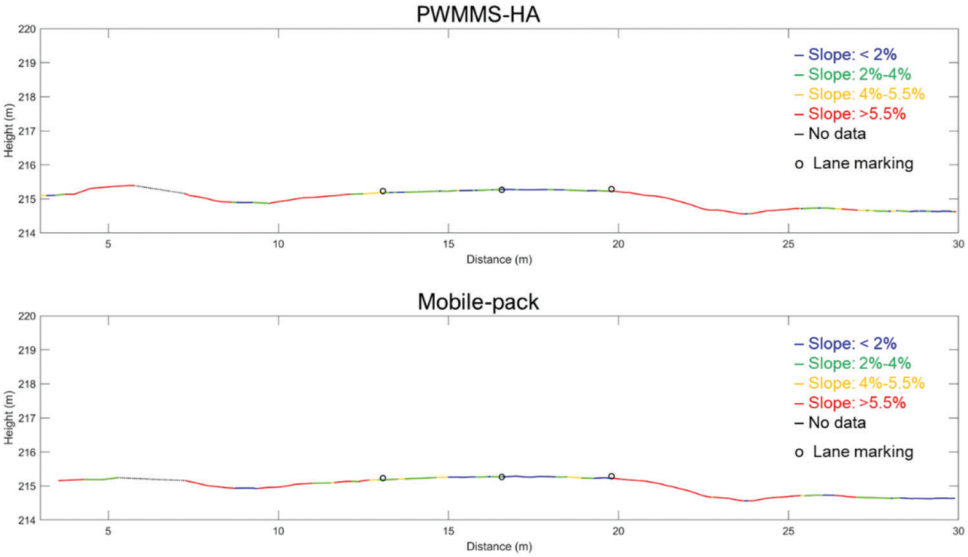

(b)

Figure 5.8 *Continued.*

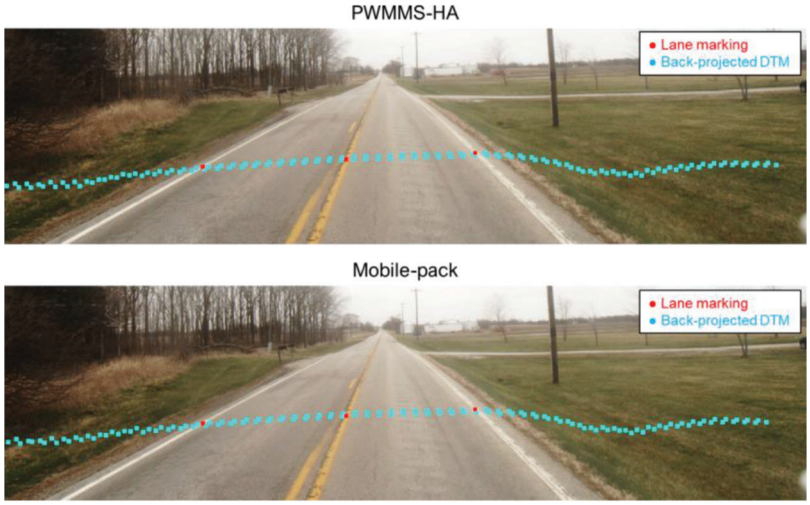

Figure 5.8 Cross-sectional profile at location PC2: (a) point cloud and DTM profiles, (b) slope evaluation results together with lane marking points, and (c) image with back-projected DTM and lane marking points. The lane marking points are extracted from the point cloud using the approach proposed by Cheng et al. (2020).

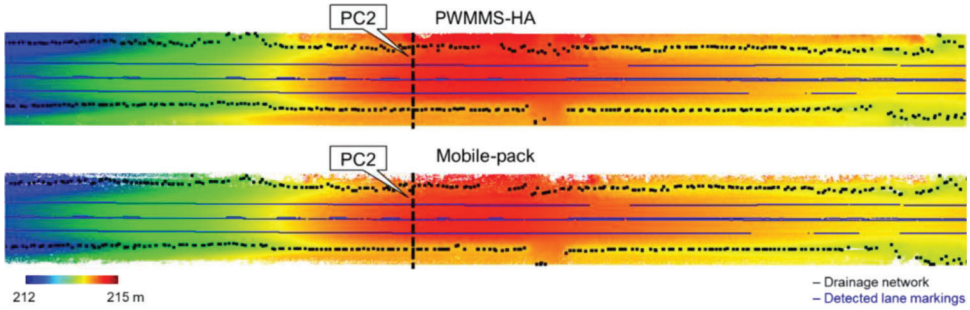

Figure 5.9 Drainage network (in black) together with detected lane markings (in blue) superimposed on the bare earth point cloud (colored by height).

able to penetrate the vegetation and capture points below canopy. The PWMMS-HA produces denser point cloud as compared to the Mobile-pack, yet the DTMs derived from both systems are compatible. The results indicate that the modified cloth simulation approach can produce a reliable terrain model as long as we have a sufficient number of points over the ROI. The slope along the profile was calculated based on the DTM points. Figure 5.8b depicts the profile PC2 colored by slope along with lane markings (detected based on the approach proposed by Cheng et al. (2020) that signify the road boundaries. The slope evaluation results from the two MLMS units are consistent with the standard values: 2% on driving lanes, 4% on shoulder, and 6-by-1 gradation for ditch lines. Figure 5.8c shows the back-projected DTM points on an image captured by the front left camera onboard the PWMMS-HA. The back-projected points coincide with the corresponding features in the image, which verifies the reliability of the system calibration.

The hydrological analyses including flow direction and flow accumulation were performed using ESRI's ArcGIS (Maidment & Morehouse, 2002). Figure 5.9 depicts the drainage network map together with the detected lane markings, using the bare earth point cloud as a base map. As can be seen in the figure, the drainage networks are aligned well with the "valley" of the ditches. Subsequently, longitudinal profiles were extracted from the drainage network by connecting major streams and removing tributaries. Figure 5.10 visualizes the longitudinal profiles and the lane markings on the left and right side of the road (when driving eastbound) where the green line, red line, and blue line are the profile from PWMMS-HA, profile from Mobile-pack, and detected lane marking, respectively. The longitudinal profiles extracted from the PWMMS-HA and Mobile-pack data are compatible as the green and red lines are almost aligned with each other. Moreover, the grade of the ditch line follows the grade of the road, and the elevation of the ditch line is consistently lower than the road centerline. Six cross-sectional profiles at locations PC1 to PC6 were also extracted and visualized in Figure 5.11, both in 3D and 2D. Profiles at locations PC1, PC2, PC3, and PC4 (see

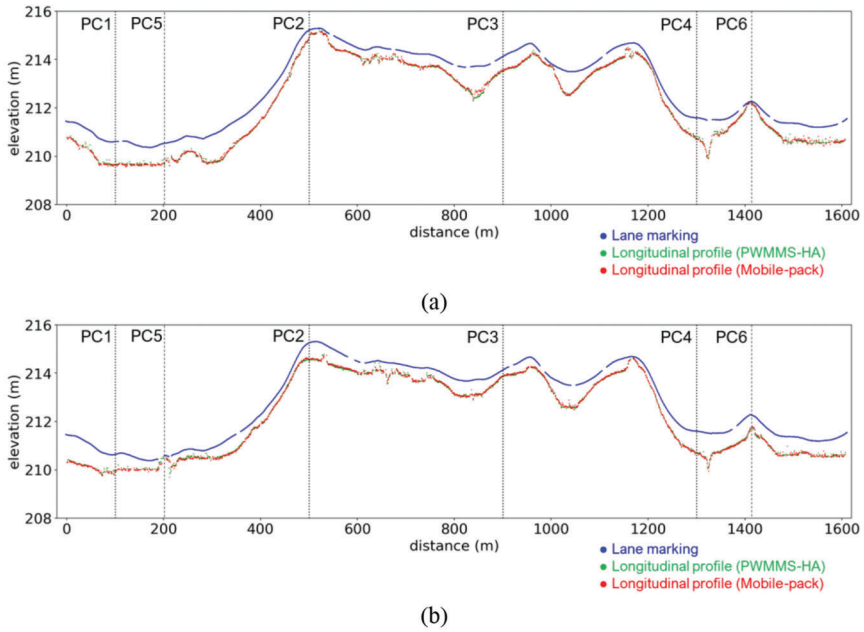

Figure 5.10 Longitudinal profiles from PWMMS-HA and Mobile-pack data together with the detected lane marking showing: (a) the ditch and road edge line on the left and (b) the ditch and road edge line on the right when driving eastbound.

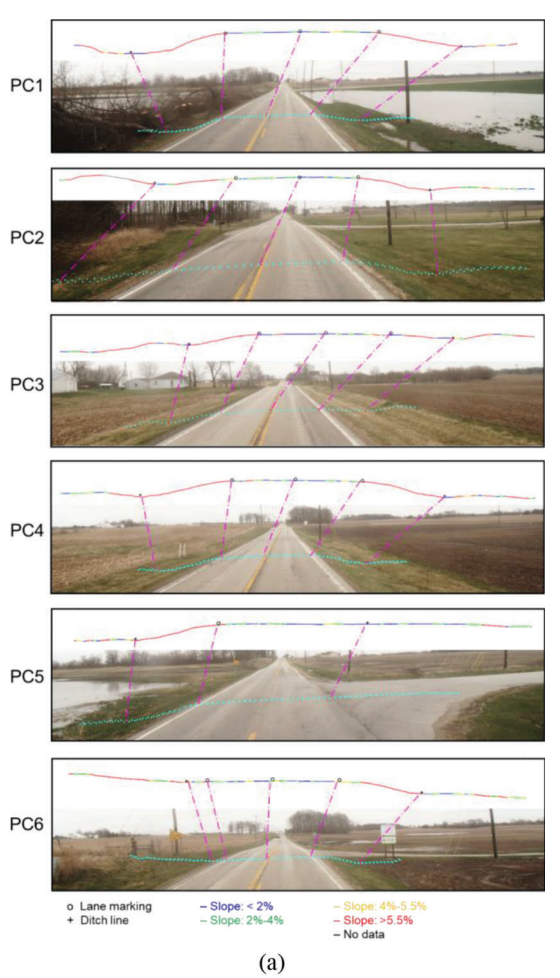

Figure 5.11 *Continued.*

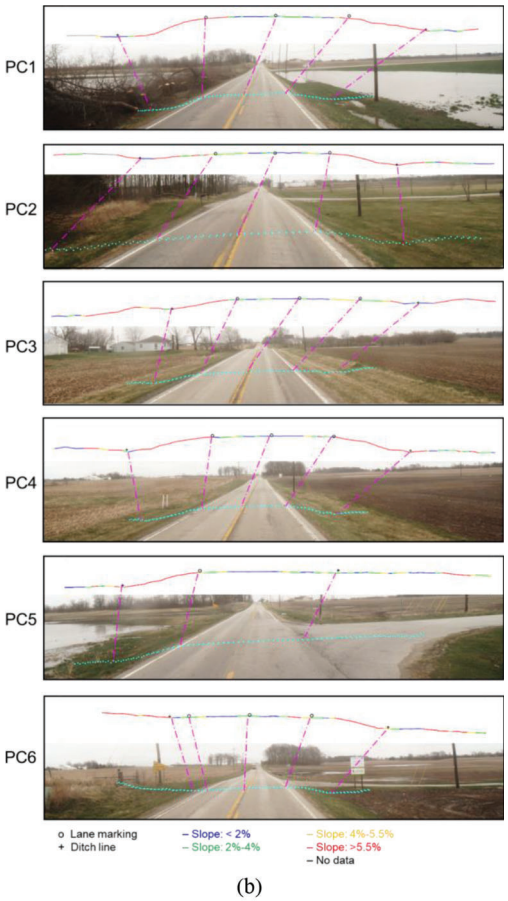

Figure 5.11 Cross-sectional profiles at locations PC1 to PC6 with links (magenta dashed lines) connecting the 3D profiles (side view and colored by slope) and the images from (a) PWMMS-HA and (b) Mobile-pack.

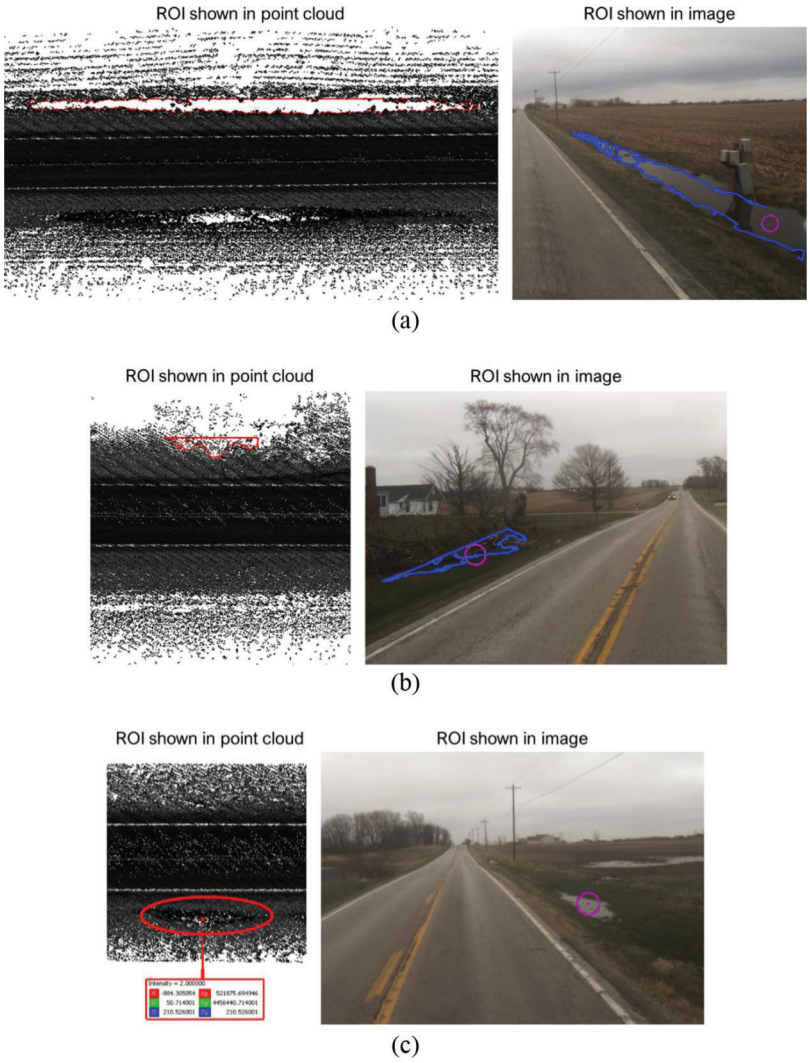

Figure 5.12 Sample potential flooded region detection results showing: (a) true positive, (b) false positive owing to occlusion by trees and (c) false negative due to the presence of LiDAR return over water bodies. The ROI is shown both in point cloud and image.

Figure 3.4) were extracted at an interval of 400 m. Locations PC5 and PC6 show areas where the elevation of the ditch line is very close to that of the road edge line, as can be seen in Figure 5.10. Based on the 2D and 3D visualization shown in Figure 5.11, location PC5 is an intersection and thus there is no ditch on the right side of the road. Location PC6 shows an area where the ditch on the left side of the road is very shallow and can barely be seen.

The strength of MLMS units for characterizing roadside ditches lies in the ability to (1) visualize the profiles in 3D point clouds as well as 2D images, and (2) incorporate other information derived from MLMS data (for example, the detected lane markings). Such capability leads to a thorough understanding of roadside drainage conditions, which is the key to prioritizing and planning maintenance. In addition, with the proposed ditch line characterization approach, the relatively low-cost system (Mobile-pack) can achieve similar performance as compared to PWMMS-HA.

Finally, the proposed water detection approach was tested on the C-1 and C-2 datasets. The area threshold was set to 1 square meter; that is, any gap with an area smaller than 1 square meter would more likely be caused by occlusions or point cloud sparsity rather than standing water. The detected flooded regions were visualized and reported in 3D point clouds as well as 2D images. Figure 5.12 shows examples of true positive, false positive, and false negative. The detection results were compared to the manually established flooded locations and the performance was evaluated and reported in Table 5.4. For both PWMMS-HA and Mobile-pack, the computed precision score is low because of the large number of false positives. The Mobile-pack, however, has a high recall score, which implies a low false negative rate.

TABLE 5.4
Performance metrics—precision and recall—of the potential flooded region detection evaluated using C-1 and C-2 datasets

	PWMMS-HA	Mobile-Pack
True Positive	7	12
False Positive	5	26
False Negative	6	1
Precision	58%	32%
Recall	54%	92%

Closer inspection of the detection results reveals that in addition to water bodies, there are other factors that can result in gaps in the bare earth point cloud. Occlusions caused by vegetation (see Figure 5.12b) are the main reason for false positives in this region of interest. The false negatives, on the other hand, are solely due to the existence of LiDAR returns from water bodies. As shown in Table 5.4, false negatives are more common in PWMMS-HA data than Mobile-pack data. One possible reason could be the different orientations of the LiDAR units. A LiDAR sensor mounted at a certain angle is likely to collect some point returns from shallow water bodies, however, such returns are unreliable for range measurements (Worstell et al., 2014). Based on the discussion above, it is a challenge to reduce the false positive rate of water detection. However, with the 2D–3D cross-visualization, an operator can quickly go through the reported areas and filter out those false positives. A high recall score is really the key, and in this case, the Mobile-pack outperforms the PWMMS-HA.

In this section, the performance of PWMMS-HA and Mobile-pack for roadside ditch characterization was evaluated. The advantage of PWMMS-HA is that the point cloud has a more uniform density and a larger coverage (up to 20 m from the road edge). That is, in addition to the roadside ditches, the PWMMS-HA point cloud can provide information on the areas adjacent to the ditches. Such information is helpful for investigating the causes of local flooding. Nevertheless, both PWMMS-HA and Mobile-pack point clouds have adequate spatial coverage for ditch line characterization. The cross-sectional profiles, drainage network, and longitudinal profiles extracted from both MLMS units are shown to be compatible. For potential flooded region detection, the Mobile-pack outperformed PWMMS-HA for its high recall score since PWMMS-HA tended to get LiDAR returns from water bodies.

6. CONCLUSIONS AND RECOMMENDATIONS FOR FUTURE WORK

This report presented an evaluation and application of mobile LiDAR in mapping roadside ditches for slope and drainage analyses. The performance of different grades of mobile LiDAR mapping systems was assessed in terms of spatial coverage, relative vertical accuracy, and absolute vertical accuracy. All the systems have complete spatial coverage over the roadside ditches with sufficient drive-runs/flight lines. Point clouds from different MLMS units, including an unmanned aerial vehicle, an unmanned ground vehicle, a portable Backpack system along with its vehicle-mounted version, a medium-grade wheel-based system, and a high-grade wheel-based system, are in agreement within a ± 3 cm range along the vertical direction. The absolute accuracy of the point cloud from different MLMS units was assessed against RTK-GNSS survey. For all the MLMS units, the absolute vertical accuracy was found to be ± 3 cm for solid surfaces and ± 7 cm for vegetated areas. Field surveys with the wheel-based and vehicle-mounted portable systems are more efficient and can be scaled up to cover a large area that is impractical with UAV, UGV, and Backpack surveys. To even a greater extent, the low cost of the vehicle-mounted portable system (as shown in Figure 6.1) in contrast to the more sophisticated platforms, the medium-grade and high-grade wheel-based systems, makes the former even more justifiable for its application in ditch line mapping.

A framework for ditch line characterization, including (1) cross-sectional profile extraction, visualization, and slope evaluation, (2) drainage network and longitudinal profile extraction, and (3) potential flooded region detection and visualization, is proposed and tested using datasets acquired by the medium-grade wheel-based and vehicle-mounted portable systems. An existing ground filtering approach, cloth simulation, is modified to handle variations in point density of the mobile LiDAR data. Drainage analysis was conducted to identify ditch lines and detect any potential drainage issues. The cross-sectional/longitudinal profiles of the ditch were automatically extracted from LiDAR data and visualized both in 2D image and 3D point cloud. The slope along the profile was calculated, reported, and compared against standard values. Potential flooded regions are identified and visualized both in point cloud and images. A recall score of 54% and 92% was achieved by the medium-grade wheel-based and vehicle-mounted portable systems, respectively. These results, when combined with other information derived from MLMS data, lead to a thorough understanding of highway conditions, which is helpful for planning highway maintenance. If multi-date datasets are available, the proposed framework can be implemented to identify changes in the 2D location as well as the elevation/slope of the ditches. This can signal the presence of sediments/debris in the ditch or the erosion of the ditch line material.

Currently, our analysis is solely based on topographic data. In the future, it is possible to incorporate weather and hydrological data, and perform flood simulation to identify areas with flooding risk. Future research will also focus on comparative analysis of mapped ditch profiles and as-built drawings, which would signify how the mapped profiles deviate from the designed profiles. Furthermore, additional information like intensity data will be utilized in the potential flooded region detection to improve the performance. Finally, for all the MLMS units discussed in this study, in particular, the vehicle-mounted portable system

(a) (b)

Figure 6.1 Photos showing field surveys with: (a) portable Backpack and (b) vehicle-mounted portable systems.

owing to its portability, one of the future activities will investigate different orientation options of the LiDAR unit to achieve an optimized coverage (and point density) of roadside ditches while maximizing the data acquisition throughput of the MLMS.

REFERENCES

Applanix. (n.d.a). *Applanix APX-15 UAV: Version 3, single board GNSS-inertial solution* [PDF Datasheet]. Retrieved April 26, 2020, from https://www.4dglobal.com.au/wp-content/uploads/2018/11/APX15_UAV.pdf

Applanix. (n.d.b). *Applanix POS LV* [PDF Datasheet]. Retrieved April 26, 2020, from https://www.applanix.com/downloads/products/specs/POS-LV-Datasheet.pdf

Ariza-Villaverde, A. B., Jiménez-Hornero, F. J., & Gutiérrez de Ravé, E. (2015). Influence of DEM resolution on drainage network extraction: A multifractal analysis. *Geomorphology*, *241*, 243–254. https://doi.org/10.1016/j.geomorph.2015.03.040

Bailly, J. S., Lagacherie, P., Millier, C., Puech, C., & Kosuth, P. (2008). Agrarian landscapes linear features detection from LiDAR: Application to artificial drainage networks. *International Journal of Remote Sensing*, *29*(12), 3489–3508. https://doi.org/10.1080/01431160701469057

Barber, C. P., & Shortridge, A. (2005). Lidar elevation data for surface hydrologic modeling: Resolution and representation issues. *Cartography and Geographic Information Science*, *32*(4), 401–410. https://doi.org/10.1559/1523040057 75194692

Bertels, L., Houthuys, R., Sterckx, S., Knaeps, E., & Deronde, B. (2011). Large-scale mapping of the riverbanks, mud flats and salt marshes of the scheldt basin, using airborne imaging spectroscopy and LiDAR. *International Journal of Remote Sensing*, *32*(10), 2905–2918. https://doi.org/10.1080/01431161003745632

Broersen, T., Peters, R., & Ledoux, H. (2017). Automatic identification of watercourses in flat and engineered landscapes by computing the skeleton of a LiDAR point cloud. *Computers & Geosciences*, *106*, 171–180. https://doi.org/10.1016/j.cageo.2017.06.003

Buchanan, B., Easton, Z. M., Schneider, R. L., & Walter, M. T. (2013). Modeling the hydrologic effects of roadside ditch networks on receiving waters. *Journal of Hydrology*, *486*, 293–305. https://doi.org/10.1016/j.jhydrol.2013.01.040

Cheng, Y.-T., Patel, A., Wen, C., Bullock, D., & Habib, A. (2020). Intensity thresholding and deep learning based lane marking extraction and lane width estimation from mobile light detection and ranging (LiDAR) point clouds. *Remote Sensing*, *12*(9), 1379. https://doi.org/10.3390/RS12091379

Fischler, M. A., & Bolles, R. C. (1981, June). Random sample consensus: a paradigm for model fitting with applications to image analysis and automated cartography. *Graphics and Image Processing*, *24*(6), 381–395.

Google. (2018a). [Google Earth Image of East 500 North, West Lafayette, IN. USA]. Google Earth. Retrieved November 17, 2021, from https://earth.google.com/web/

Google. (2018b). [McCormick Rd, West Lafayette, IN, USA]. Google Earth. Retrieved November 17, 2021, from https://earth.google.com/web/

Google. (2018c). [State Rd 28, Washington Township, IN, USA]. Google Earth. Retrieved November 17, 2021, from https://earth.google.com/web/

Günen, M. A., Atasever, Ü. H., Taşkanat, T., & Beşdok, E. (2019). Usage of unmanned aerial vehicles (UAVs) in determining drainage networks. *Nature Sciences*, *14*(1), 1–10. Retrieved from https://dergipark.org.tr/en/pub/nwsanature/issue/42897/427665

Habib, A., Lay, J., & Wong, C. (2006). *LIDAR error propagation calculator* [Zip file]. https://engineering.purdue.edu/CE/Academics/Groups/Geomatics/DPRG/files/LIDARErrorPropagation.zip

Habib, A., & Lin, Y.-J. (2016). Multi-class simultaneous adaptive segmentation and quality control of point cloud data. *Remote Sensing*, *8*(2), 104. https://doi.org/10.3390/rs8020104

Hexagon. (n.d.a). *Novatel SPAN-CPT*. Retrieved May 26, 2021, from https://novatel.com/support/previous-generation-products-drop-down/previous-generation-products/span-cpt

Hexagon. (n.d.b). *Novatel SPAN-IGM-A1*. Retrieved May 26, 2021, from https://novatel.com/support/span-gnss-inertial-navigation-systems/span-combined-systems/span-igm-a1

Hexagon. (2021, July). *Novatel IMU-ISA-100C*. Retrieved April 26, 2020, from https://docs.novatel.com/OEM7/Content/Technical_Specs_IMU/ISA_100C_Overview.htm

Ibeh, C., Pallai, C., & Saavedra, D. (n.d.). *Lidar-based roadside ditch mapping in York and Lancaster Counties, Pennsylvania* [PDF file]. Conservative Innovation Center. https://www.chesapeakebay.net/documents/Lidar-Based_Roadside_Ditch_Mapping_Report.pdf

Jenson, S. K., & Domingue, J. O. (1988). Extracting topographic structure from digital elevation data for geographic information system analysis. *Photogrammetric Engineering and Remote Sensing*, *54*(11), 1593–1600.

Levavasseur, F., Bailly, J. S., Lagacherie, P., Colin, F., & Rabotin, M. (2012). Simulating the effects of spatial

configurations of agricultural ditch drainage networks on surface runoff from agricultural catchments. *Hydrological Processes*, *26*(22), 3393–3404.

Levavasseur, F., Lagacherie, P., Bailly, J. S., Biarnès, A., & Colin, F. (2015). Spatial modeling of man-made drainage density of agricultural landscapes. *Journal of Land Use Science*, *10*(3), 256–276. https://doi.org/10.1080/1747423X.2014.884644

Lin, Y. C., Cheng, Y.-T., Lin, Y.-J., Flatt, J. E., Habib, A., & Bullock, D. (2019). Evaluating the accuracy of mobile LiDAR for mapping airfield infrastructure. *Transportation Research Record: Journal of the Transportation Research Board*, *2673*(4), 117–124. https://doi.org/10.1177/0361198119835802

Lin, Y.-C., & Habib, A. (2021). Quality control and crop characterization framework for multi-temporal UAV LiDAR data over mechanized agricultural fields. *Remote Sensing of Environment*, *256*, 112299. https://doi.org/10.1016/j.rse.2021.112299

Maidment, D. R., & Morehouse, S. (2002). *Arc Hydro: GIS for water resources*. ESRI Inc.

McGee, H. W., Nabors, D., & Baughman, T. (2009, July). *Maintenance of drainage features for safety: A guide for local street and highway maintenance personnel* (Report No. FHWA-SA-09-024). U.S Department of Transportation Federal Highway Administration. https://clgt.okstate.edu/site-files/docs/fhwamaintdrain4safety.pdf

Metz, M., Mitasova, H., & Harmon, R. S. (2011). Efficient extraction of drainage networks from massive, radar-based elevation models with least cost path search. *Hydrology and Earth System Sciences*, *15*(2), 667–678. https://doi.org/10.5194/hess-15-667-2011

Murphy, P. N. C., Ogilvie, J., Meng, F.-R., & Arp, P. (2007). Stream network modelling using lidar and photogrammetric digital elevation models: a comparison and field verification. *Hydrological Processes*, *22*, 1747–1754. https://doi.org/10.1002/hyp.6770

Pricope, N. G., Halls, J. N., Mapes, K. L., Baxley, J. B., & Wu, J. J. (2020). Quantitative comparison of UAS-borne lidar systems for high-resolution forested wetland mapping. *Sensors (Switzerland)*, *20*(16), 4453. https://doi.org/10.3390/s20164453

Rapinel, S., Hubert-Moy, L., Clément, B., Nabucet, J., & Cudennec, C. (2015). Ditch network extraction and hydrogeomorphological characterization using LiDAR-derived DTM in wetlands. *Hydrology Research*, *46*(2), 276–290. https://doi.org/10.2166/nh.2013.121

Ravi, R., & Habib, A. (in press). Least squares adjustment with a rank-deficient weight matrix and its applicability towards image/LiDAR data processing. *Photogrammetric Engineering & Remote Sensing*.

Ravi, R., Habib, A., & Bullock, D. (2020). Pothole mapping and patching quantity estimates using LiDAR-based mobile mapping systems. *Transportation Research Record*, *2674*(9), 124–134. https://doi.org/10.1177/0361198120927006

Ravi, R., Lin, Y.-J., Elbahnasawy, M., Shamseldin, T., & Habib, A. (2018). Simultaneous system calibration of a multi-LiDAR multi-camera mobile mapping platform. *IEEE Journal of Selected Topics in Applied Earth Observations and Remote Sensing*, *11*(5), 1694–1714. https://doi.org/10.1109/JSTARS.2018.2812796

Renaudin, E., Habib, A., & Kersting, A. P. (2011). Featured-based registration of terrestrial laser scans with minimum overlap using photogrammetric data. *ETRI Journal*, *33*(4), 517–527. https://doi.org/10.4218/etrij.11.1610.0006

Riegl. (n.d.). *Riegl VUX-1HA* [Webpage]. Retrieved April 26, 2020, from http://www.riegl.com/nc/products/mobile-scanning/produktdetail/product/scanner/50/

Roelens, J., Höfle, B., Dondeyne, S., Van Orshoven, J., & Diels, J. (2018). Drainage ditch extraction from airborne LiDAR point clouds. *ISPRS Journal of Photogrammetry and Remote Sensing*, *146*(December 2018), 409–420. https://doi.org/10.1016/j.isprsjprs.2018.10.014

Roelens, J., Rosier, I., Dondeyne, S., Van Orshoven, J., & Diels, J. (2018). Extracting drainage networks and their connectivity using LiDAR data. *Hydrological Processes*, *32*(8), 1026–1037. https://doi.org/10.1002/hyp.11472

Schneider, R., Orr, D., & Johnson, A. (2019). Understanding ditch maintenance decisions of local highway agencies for improved water resources across New York State. *Transportation Research Record: Journal of the Transportation Research Board*, *2673*(12), 767–773. https://doi.org/10.1177/0361198119854092

Suzuki, S., & Be, K. (1985, April). Topological structural analysis of digitized binary images by border following. *Computer Vision, Graphics, and Image Processing*, *30*(1), 32–46. https://doi.org/10.1016/0734-189X(85)90016-7

Velodyne Lidar. (n.d.a). *Velodyne HDL32E datasheet*. Retrieved May 26, 2021, from https://velodynelidar.com/products/hdl-32e/

Velodyne Lidar. (n.d.b). *Velodyne Puck Hi-Res datasheet*. Retrieved May 26, 2021, from https://velodynelidar.com/products/puck-hi-res/

Velodyne Lidar. (n.d.c). *Velodyne Ultra Puck datasheet*. Retrieved May 26, 2021, from https://velodynelidar.com/products/ultra-puck/

Wen, C., Sun, X., Li, J., Wang, C., Guo, Y., & Habib, A. (2019). A deep learning framework for road marking extraction, classification and completion from mobile laser scanning point clouds. *ISPRS Journal of Photogrammetry and Remote Sensing*, *147*(January 2019), 178–192. https://doi.org/10.1016/j.isprsjprs.2018.10.007

Worstell, B. B., Poppenga, S. K., Evans, G. A., & Prince, S. (2014). *Lidar point density analysis: Implications for identifying water bodies* (Scientific Investigations Report 2014–5191). U.S. Geological Survey. http://dx.doi.org/10.3133/sir20145191

Zhang, W., Qi, J., Wan, P., Wang, H., Xie, D., Wang, X., & Yan, G. (2016). An easy-to-use airborne LiDAR data filtering method based on cloth simulation. *Remote Sensing*, *8*(6), 501. https://doi.org/10.3390/rs8060501

Zoller + Frolich. (n.d.). *Z+F Profiler 9012*. Retrieved April 26, 2020, from https://www.zf-laser.com/Z-F-PROFILER-R-9012.2d_laserscanner.0.html

About the Joint Transportation Research Program (JTRP)

On March 11, 1937, the Indiana Legislature passed an act which authorized the Indiana State Highway Commission to cooperate with and assist Purdue University in developing the best methods of improving and maintaining the highways of the state and the respective counties thereof. That collaborative effort was called the Joint Highway Research Project (JHRP). In 1997 the collaborative venture was renamed as the Joint Transportation Research Program (JTRP) to reflect the state and national efforts to integrate the management and operation of various transportation modes.

The first studies of JHRP were concerned with Test Road No. 1—evaluation of the weathering characteristics of stabilized materials. After World War II, the JHRP program grew substantially and was regularly producing technical reports. Over 1,600 technical reports are now available, published as part of the JHRP and subsequently JTRP collaborative venture between Purdue University and what is now the Indiana Department of Transportation.

Free online access to all reports is provided through a unique collaboration between JTRP and Purdue Libraries. These are available at http://docs.lib.purdue.edu/jtrp.

Further information about JTRP and its current research program is available at http://www.purdue.edu/jtrp.

About This Report

An open access version of this publication is available online. See the URL in the citation below.

Habib, A., Bullock, D. M., Lin, Y.-C., & Manish, R. (2021). *Road ditch line mapping with mobile LiDAR* (Joint Transportation Research Program Publication No. FHWA/IN/JTRP-2021/26). West Lafayette, IN: Purdue University. https://doi.org/10.5703/1288284317354